Relaxor Properties of Doped $BaTiO_3$ Ferroelectrics

By

Zaka Ullah

DEPARTMENT OF PHYSICS
QUAID-I-AZAM UNIVERSITY
ISLAMABAD, PAKISTAN
2016

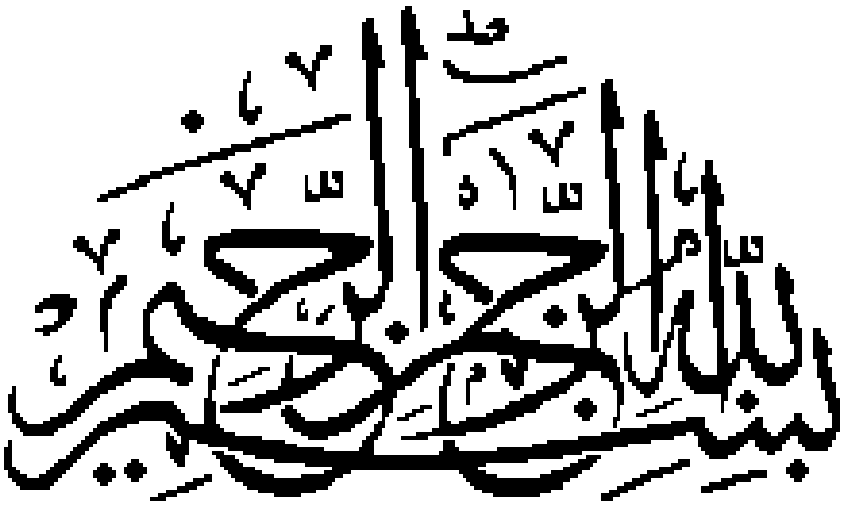

In the name of Allah,
Most Gracious, Most
Merciful.

This work is submitted as a dissertation
In partial fulfillment of the requirement for the degree of

MASTER OF PHILOSOPHY
IN
PHYSICS

To The

Department of Physics
Quaid-i-Azam University
Islamabad, Pakistan

2016

CERTIFICATE

This is to certify that the experimental work in this dissertation has been carried out by ***Mr. Zaka Ullah*** under my supervision in the Superconductivity and Magnetism Lab, Department of Physics, Quaid-i-Azam University, Islamabad, Pakistan.

Supervisor:

Dr. Arif Mumtaz
Professor
Department of Physics
Quaid-i-Azam University
Islamabad, Pakistan.

Submitted Through:

Prof. Dr. Arshad Majid Mirza
Chairman
Department of Physics
Quaid-i-Azam University
Islamabad, Pakistan.

DEDICATION

To
My Parents
&
My Supervisor

ACKONWLEDGEMENTS

*All praise be to **Allah**, the Cherisher and Sustainer of the worlds, the most beneficent and merciful, who gave me strength to achieve what I wanted to and blessed me all the ways. Many peace and blessings be upon the Seal of the **Prophet Muhammad (SAW)**, the most perfect and splendid.*

*Foremost, I would like to express my deep sense of gratitude to my advisor **Prof. Dr. Arif Mumtaz** for his immense help, guidance and encouragement throughout my research. I really owe him for his keen interest in my research despite his busy schedule.*

*I am also immensely grateful to **Dr. S. K. Hasanain** for his support in providing encourages, guidance and good teaching. He is ideal teacher for me during my entire academic years.*

*I avail this opportunity to express my deep sense of gratitude to **Dr. Ghulam Hassnain Jaffri** for his cooperation in one way or the other during my entire M.Phil. Session. I owe a noteworthy debt to him for providing encouragement and guidance.*

*With deep regards and profound respect, I am deeply indebted to **Dr. Muhammad Usman** for his valuable ideas, encouragement, sound advice, good company, lots of good concepts and a confidence to handle FURNACES, XRD and PLD. He has always been my prime resource and inspiration. He has always put great efforts to explain things clearly and simply, and without his attention this thesis would likely not have developed.*

*I offer my sincere thanks and gratitude to **Dr. Shahzad, Asad bhai and Adnan Tahir** for thier cooperation in one way or the other during my entire M.Phil. Session.*

*I am also thankful to all my Lab fellows **Bilal, Ateeq, Qasim, Umer, Khalid and Sadaf**, for the moral support and for creating a comfortable working environment.*

*Leaving the personal until last, I am exceedingly grateful to my parents, **Mr. & Mrs. Muhammad Aslam khan** for their endless love, support, and sacrifice from the very first day of my journey of life. They provided me with the ability and opportunities to follow my dreams. I am thanking my beloved brothers **(Asad, Faseeh, Abd Ullah and Abdur Rehman)** and Sisters for all the hope, true love, affection, caring, concern and constant encouragement.*

*I am deeply indebted to my all friends especially **(Usman, Shafqat , Zahoor, Atif, Adnan, Arif, saleem. Laiq zia and Khurram Tariq)** and all cousins especially **(Haroon,***

Hummayun, Tauseef, Noman. Usama, Hamza and Mudassir) *for their continuously cooperation and moral support.*

Words can never express my feelings. I acknowledge every person in my life who have always been there for me in every thick and thin condition and braced me making my M. Phil possible.

ABSTRACT

Perovskite type $Ba_{1-x}Sr_xZr_{0.2}Ti_{0.8}O_3$ (with x = 0.0, 0.1, 0.2 and 0.3) and $Ba_{1-x}Sr_xZr_{0.3}Ti_{0.7}O_3$ (with x = 0.0, 0.1, 0.2, 0.24, 0.27 and 0.3) ceramics have been synthesized through conventional two step solid state reaction method. The Structural Characterization were investigated using room temperature X-ray diffraction study. All the compositions reveal a single phase cubic structure. The dielectric measurements were taken at various temperature (100 K to 300 K), and at various frequencies (1 kHz to 500 kHz) for all the prepared compositions. This study reveals that the $Ba_{1-x}Sr_xTi_{0.8}Zr_{0.2}O_3$ (with x = 0.0, 0.1, 0.2 and 0.3) composition does not transform from normal ferroelectric to relaxor ferroelectric while $Ba_{1-x}Sr_xTi_{0.7}Zr_{0.3}O_3$ (with x = 0.0, 0.1, 0.2, 0.24, 0.27 and 0.3) compositions are of relaxor type and undergo a diffuse type ferroelectric phase transition. The diffusivity increases with increase in Sr concentration in the present composition range. It is observed that with increase in Sr concentration the transition temperature decreases for all the studied compositions. This may occur due to the introduction of smaller ionic radius of Sr^{+2} at the site of larger ionic radius of Ba^{+2}. It is also observed that with increase in Sr content the maxima of dielectric constant increases for all studied compositions of $Ba_{1-x}Sr_xTi_{0.8}Zr_{0.2}O_3$ (with x = 0.0, 0.1, 0.2 and 0.3). However, for $Ba_{1-x}Sr_xTi_{0.7}Zr_{0.3}O_3$ the dielectric constant maxima increases up to x = 0.24 and then further increment in Sr content up to x= 0.3, the maxima of dielectric constant shows decrease.

Contents

List of Figures

List of Tables

Chapter 1 INTRODUCTION

1.1 Introduction

Barium titanate (BTO), abbreviated BT, based materials have been widely studied for their interesting properties like high dielectric constant, low dielectric loss, practical piezoelectric and pyroelectric behavior. Since the discovery of the applications of $BaTiO_3$ (BT), several A-site and B site isovalent substituted compositions have been studied [1] such as $ATiO_3$ and $BaBO_3$ where A=Ca, Sr, Pb, Mn and B=Zr, Sn, Hf, Mn [2]. Among this isovalent substitution most of the research are done on Sr at A site and Zr at B site of the BT pervoskites. Sr^{2+} (0.144 nm) and Zr^{4+} (0.072 nm) have similar ionic radii that of Ba^{2+} (0.161 nm) and Ti^{4+} (0.061 nm) respectively. Thus, $BaTiO_3$ simply forms complete solid solutions with $SrTiO_3$ and $BaZrO_3$. Barium strontium titanate $(Ba,Sr)TiO_3$ (BST) with high dielectric constant value joined with low dissipation factor makes BST one of the favourable candidates for dynamic random access memory (DRAM) applications. The BST system is famous for its strong response to the applied dc electric field. This property is very attractive and has been used for advance devices operating in the microwave and millimeter range such as phase shifters, frequency agile filters, and tunable capacitors. Moreover, the substitution of barium by strontium in barium titanate can improve the properties such as lowering the temperature of ferroelectric transformation, increasing dielectric constant, lowering dielectric dissipation and elevating pyroelectric coefficient. It is also reported that barium zirconate titanate (BZT) solid solutions are also electric field-tunable dielectrics with potential use in devices for wireless communications as variable capacitors, phase shifters and voltage-controlled oscillators. There are lots of reports on the compositional modified solid solution of $BaTiO_3$ and $BaZrO_3$. Most of the research was focused on temperature dependence of the dielectric properties for capacitor applications. The dielectric and ferroelectric properties of BZT are largely dependent on the amount of Zr substitution [1, 2]

1.2 Ferroelectrics

Ferroelectric materials possess spontaneous electric polarization and can be reversed in a presence of external applied electric field. The ferroelectricity is analogous to the materials which show ferromagnetism (due to the permanent magnetic moment). This phenomenon can be explained as, there is a slight imbalance between a positive and

negative charges in the ferroelectric crystal which in turn act as an electric dipole and that's why the ferroelectric materials possess electric dipole moment even if there is no external applied Electric field [3]. The other main and prominent feature of ferroelectric material is, that they exhibit hysteresis between the polarization and the field (electric) [4, 5].

1.2.1 Ferroelectric Crystal Structure

The majority of the valuable ferroelectrics have the perovskite (ABO_3) crystal structure shown in figure 1.1. The basic perovskite structure is cubic, where A (Na^{+2}, Ba^{+2}, Ca^{+2}, Sr^{+2} etc.) represent the cation (large) at the cube corners, B (Ti^{+4}, Zr^{+4}, Sn^{+4}, etc.) represent the cation (small) at the body centre position and O represent oxygen at the face centred positions.

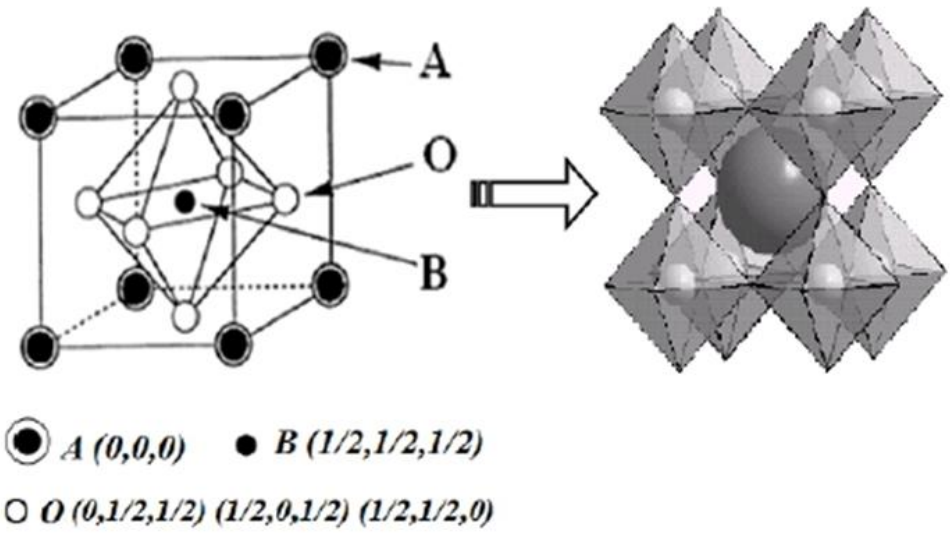

Figure 1.1: The typical perovskite structure of ABO_3. B ion is surrounded by six oxygen atoms.

There are many ferroelectric as well as piezoelectric ceramics like barium titanate ($BaTiO_3$),barium strontium titanate ($Ba_{1-x}Sr_xTiO_3$) lead titanate ($PbTiO_3$), lead zirconate titanate ($PbZr_xTi_{1-x}O_3$), potassium niobate ($KNbO_3$), potassium sodium niobate ($K_xNa_{1-x}NbO_3$), lead lanthanum zirconate titanate (PLZT) have the perovskite structure [6, 7].

1.2.2 Ferroelectric domains and hysteresis loop

Ferroelectric material contain a large number of intrinsic electric dipoles which are randomly oriented and hence the material as a whole dose not possess any polarization. On

a small scale there are ferroelectric domains formation take place where dipoles show a uniform polarization. In a particular domain the electric dipoles have same direction. The domains are separated by a boundaries (interfaces) called domain walls. So the domains (having net polarization in a specific direction) aligned in such a way that as a whole material is un-polarized when there is no external applied electric field present. When the field is applied the domain align themselves in a direction of applied field and the material possess a strong polarization as shown in fig.1.2 [6, 8].

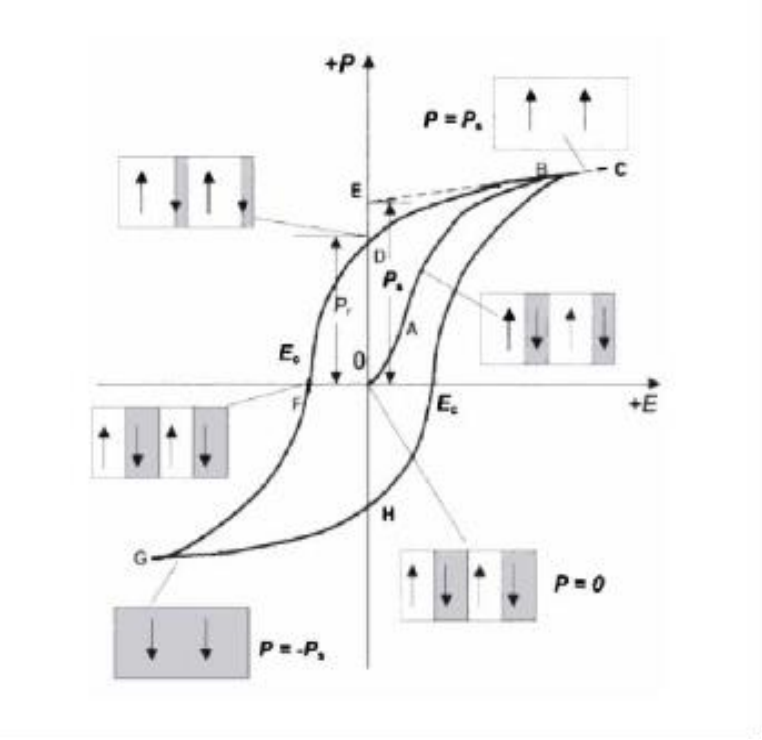

Figure 1.2: Typical P vs E hysteresis loop of ferroelectric.

The figure 1.2 clearly indicates that application of an electric field to a usual ferroelectric sample initiates the growth of domains in the direction of applied electric field. The polarization achieve its saturation level ($\boldsymbol{P_S}$) for efficiently high electric fields. The ferroelectric materials keep remnant polarization (P_r) even if the field is reduced to zero. On the opposite direction of field, firstly the polarization is reversed to zero and then alter its direction as the field produces saturation polarization in the reverse direction. The whole cycle of an alternating electric field gives rise to a hysteresis loop (Figure 1.2) between polarization and external applied electric field. The field at which polarization vanish (become zero) is called the coercive field ($\boldsymbol{E_C}$) [9].

1.3 Classification of materials

There are 32 different classes of crystalline materials. Out of the 32 crystal classes (i.e. point groups), 11 have a Centre of symmetry and as a result cannot exhibit polar properties. The remaining 21 are non-centrosymmetric and therefore can keep one or more polar axes. Of these, 20 classes are piezoelectric (the one leaving out being cubic class) (figure 1.3). Piezoelectric crystals possess the feature that the application of mechanical stress induces polarization, and equally, the application of an electric field yields mechanical deformation. Out of the 20 piezoelectric classes, 10 possess a unique polar axis and so are instinctively polarized, i.e. polarized when there is no applied electric field. Such crystals are called pyroelectric.

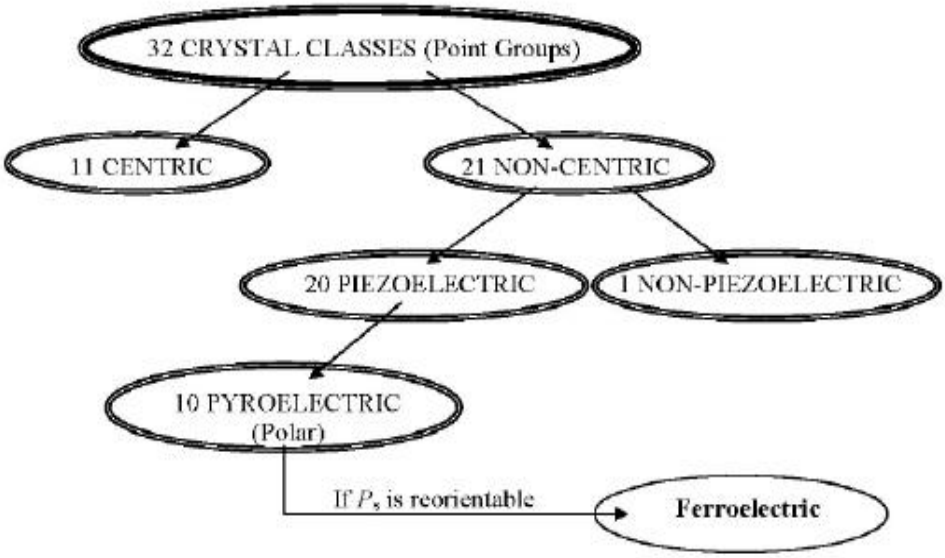

Figure 1.3: A classification scheme for 32 point groups of crystallography.

The intrinsic polarization is a function of temperature, so the natural moment in these crystals is usually achievable to observe by fluctuating the temperature, thus the name pyroelectrics. Ferroelectric crystals, a limited group of pyroelectric family, also exhibit the additional characteristic that the direction of the spontaneous polarization can be overturned (reoriented) on application of an applied electric field. Hence, every single ferroelectric is pyroelectric and piezoelectric but the entire piezoelectric are not pyroelectric and all pyroelectrics are not ferroelectric [9-11].

1.4 Goldschmidt's Tolerance Factor

Goldschmidt reported some initial research on perovskite materials using an ionic radii model and established a semi-empirical relationship known as Goldschmidt's tolerance factor that is expressed as:

$$t = \frac{r_A + r_O}{\sqrt{2}(r_B + r_O)} \quad \textbf{1.1}$$

Where r_A, r_B and r_O are the ionic radii of the corresponding A-site, B-site, and O-site, in the perovskite structure. . It has been reported in Goldschmidt's formalism for the perovskite structure that the stability of the perovskite structure may be expected to found within the limit of $0.77<t<1.05$, where the "ideal" cubic perovskite formation for t ~1.00 [10], for t < *1* often have a low symmetry distortion of the unit cell with ferroelectric rhombohedral or monoclinic phases. In situation of t >1, the material is often related with high dielectric (ferroelectric) material. Goldschmidt's tolerance factor has been using since for decades lead to discovery and advancement of perovskites, and still using by the scientific community for progressing of new perovskite materials [12].

1.5 Barium titanate

The chemical formula of barium titanate is $BaTiO_3$ and having a perovskite structure (with A=Ba and B=Ti of ABO_3 type perovskite material). It attracts much attention because of its high tenability, high dielectric permittivity and low dielectric loss at room temperature. $BaTiO_3$ is lead-free (non-toxic) ferroelectric material and so it is environmental friendly which make it a more suitable material for various applications.

$BaTiO_3$ possess four crystal structures at specific temperature called Curie temperature (transition temperature). Out of four the one (cubic) structure is paraelectric phase of $BaTiO_3$. The rest of the three (tetragonal, orthorhombic and rhombohedral) structures are in ferroelectric phase as shown in the figure [13-16].

At Curie temperature $\boldsymbol{T_C}$ the material goes through a transition from *paraelectric* (PE) to a *ferroelectric* (FE) phase. The structure symmetry of ferroelectric is lowly than the corresponding paraelectric structure. At $T > T_C$ the crystal does not show ferroelectricity, although for $T < T_C$ it is ferroelectric. In the case of more than one ferroelectric phases (e.g. in $BaTiO_3$) as shown in figure 1.4, the temperature upon which the ferroelectric crystal transforms from one phase to another is called the transition temperature [9, 10, 17].

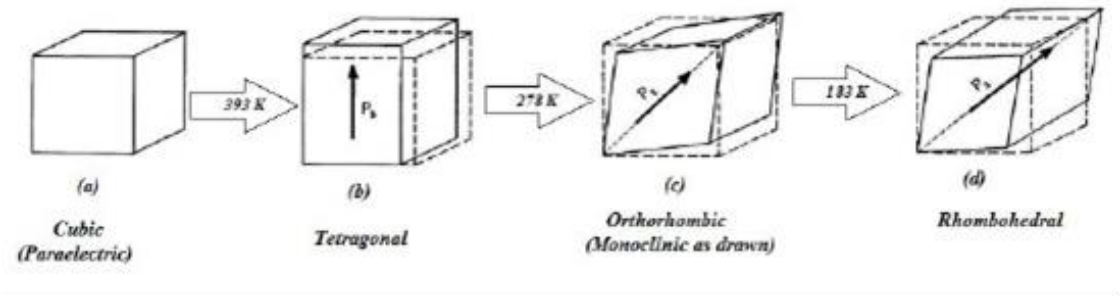

Figure 1.4: Structural transitions in BaTiO3 unit cell: a) Cubic above 393 K (TC) b) Tetragonal, 393 >T > 278 K, c) Orthorhombic, 278 > T > 183 K, d) Rhombohedral, T < 183K. Arrows indicates the direction of the spontaneous polarization

The dielectric constant of $BaTiO_3$ ferroelectric crystal show variations with temperature as it cool down from its paraelectric (non ferroelectric) cubic phase to the ferroelectric tetragonal, orthorhombic, and rhombohedral phases figure 1.5. Near the phase transition temperatures, thermodynamic properties containing dielectric, elastic, optical, and thermal constants show an anomalous behaviour. This is due to a distortion in the crystal as the phase changes [18].

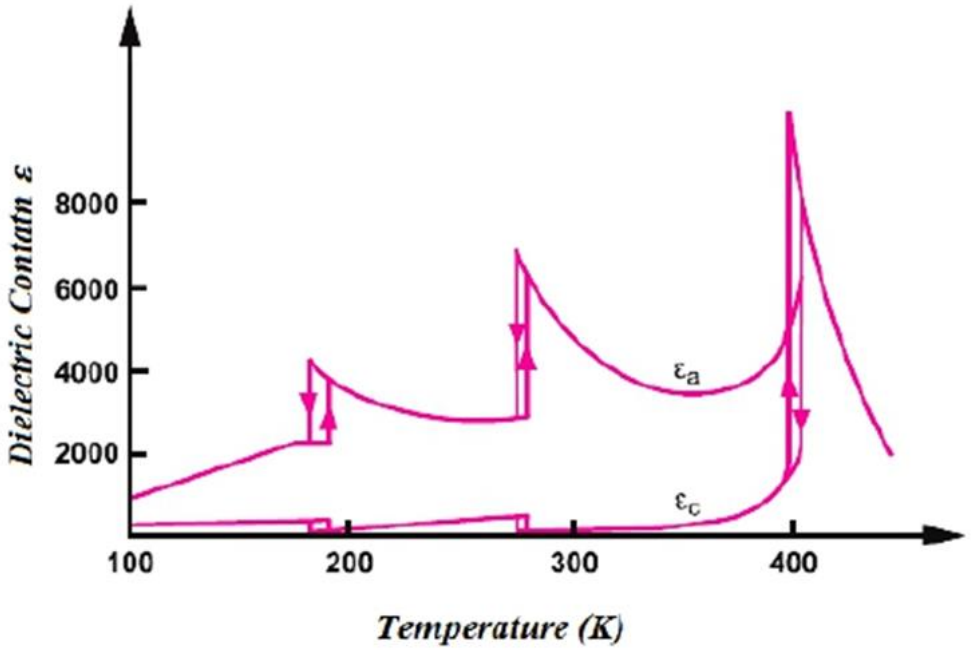

Figure 1.5: Relative permittivities measured along the 'a' and 'c' axis of a poled tetragonal $BaTiO_3$ crystal vs temperature.

1.6 Curie-Weiss law

In most ferroelectric which have multiple ferroelectric phases,the temprature at which the phase transform from one to another is called transition temrature(T_m). The dielectric constant (ε') of a ferroelectric material as a function of temprature, follow the Curie-Weiss law above the transition (curie) temprature and expressed as [19]:

$$\frac{1}{\varepsilon} = \frac{(T - Tcw)}{C} \qquad \textbf{1.2}$$

Where C and T_{CW} in the equation 1.2 are called Curie constant and Curie temperature, respectively. The Curie-Weiss temperature T_{CW} is generally dissimilar from the Curie point T_C. Curie point is the exact temperature of the transition from ferroelectric to paraelectric state and right conversely. For a first order phase transition T_C is higher than T_{CW} whereas in a second order phase transition the two are same (i.e. $T_C = T_{CW}$) [20, 21]. Curie-Weiss law comportment is one of the prime feature of ferroelectricity and has been used to mark obvious the presence of ferroelectricity in a material by many scientists. Briefly, the Curie-Weiss law is a characteristic of ferroelectrics, whereas the ability to reorient the spontaneous polarization is a necessary provision for ferroelectricity.

1.7 Classification of Ferroelectric Crystal

At first Ferroelectric materials were mostly considered into two categories on the basis of temperature variation of dielectric constant or Curie constant C: (a) soft (KH_2PO_4-type) and (b) hard ($BaTiO_3$-type).The phase transition in soft (H-bonded) ferroelectrics is of order disorder type while in hard ferroelectrics it is displacive type. In displacive type of transition a slight atomic displacement of some of the atoms is typically responsible for phase transition, which has been found in some of the perovskites. The character of ferroelectrics is specified in terms of the dynamics of phase transition.

1.8 Diffuse Phase Transition

The phase transition in which transition temperature is not distinct rather it surrounds a certain temperature interval and as a result a slow change of physical properties in this temperature section, is called diffuse phase transition (DPT). The most significant examples of DPT are found in ferroelectric materials [22, 23], even though this

phenomenon is observed in a number of types of materials [24]. Some uniqueness of the DPT are:

a. Broadened maxima in the permittivity- temperature curve.
b. Slow decrease of spontaneous and remnant polarizations with going up temperature.
c. Transition temperatures achieved by different techniques which do not overlap.
d. Relaxation character of the dielectric properties in transition region and
e. Curie-Weiss behavior is not obeyed in certain temperature intervals beyond the transition temperature.

The diffuseness of the phase transition is supposed to be due to the existence of compositional and polarization (structural) variation in a relatively large temperature interval around the transition. Polarization variation is due to the small energy change between high and low temperature phases around the transition. Complex perovskite type ferroelectrics with distorted cation arrangements show DPT which is characterized by a broad maximum for the temperature dependence of dielectric constant (ε′) and dielectric dispersion in the transition region [25, 26]. For DPT ε′ follows modified Curie Weiss behavior as follows:

$$\frac{1}{\varepsilon'} = \frac{1}{\varepsilon'_m} + \frac{(T - T'_m)^{\gamma}}{C_1} \qquad (1 \le \gamma \le 2) \qquad \textbf{1.3}$$

Where T'_m is the temperature at which ε′ extents maximum, ε'_m is the value of ε′ at T'_m, C_1 is the modified Curie Weiss like constant and γ is the critical exponent, describes the diffusivity of the materials, which lies in the range $1< \gamma <2$ [27]. The smeared out ε′ vs. T response has generally been attributed [7, 26, 28] to the occurrence of nanoregions with local compositions changing from the average composition over length scale of 100 to 1000 Å. The transition of different microregions in a macroscopic sample are assumed [7] to at different temperatures, so-called Curie range, leading DPT which is due to compositional variations. The dielectric and mechanical properties of FE structure under their T_C are functions of the state of polarization and stress.

1.9 Relaxor Ferroelectric

1.9.1 Introduction

Relaxation means a system's tedious approach to the equilibrium state after some excitation. In a case of the dielectric relaxation one should assume the response of polarization to an externa electric field, usually a small electric field. A type of disorder ferroelectrics representing peculiar structure and the properties are known as Relaxor ferroelectric or relaxors. At sufficiently high temperature they present/exists in a non-polar paraelectric phase which is same as a paraelectric phase of normal ferroelectrics. Upon lowering the temperature they change into ergodic relaxor state in which Polar Regions of nanometer size with randomly spread directions of dipole moments reveals. The temperature upon which the transformation takes place is called Burn's temperature (T_B). At temperature near to T_B polar nano regions (PNR) are mobile (moveable) and their behavior is ergodic. Upon cooling, their motion slows down extremely and at low temperature, T_f (freezing temperature) the PNR become frozen. Freezing of the dipoles motion is related with a large and wide peak in the temperature dependence of the dielectric constant (ε') and also a strong characteristic dispersion detected at all frequencies. The maximum dielectric permittivity is same as at Tc in normal ferroelectric perovskites, but in slight disagreement with normal ferroelectric it is extremely diffusive and its temperature T_m ($> T_f$) shifts with frequency due to dielectric dispersion. Because of the diffuseness in the dielectric anomaly relaxors are often called "ferroelectrics with diffuse phase transition" though no structural transition really occurs. Compositional disorder is a usual feature of relaxors i.e. the disorder in the positioning of different ions on the crystallographic positions [29].

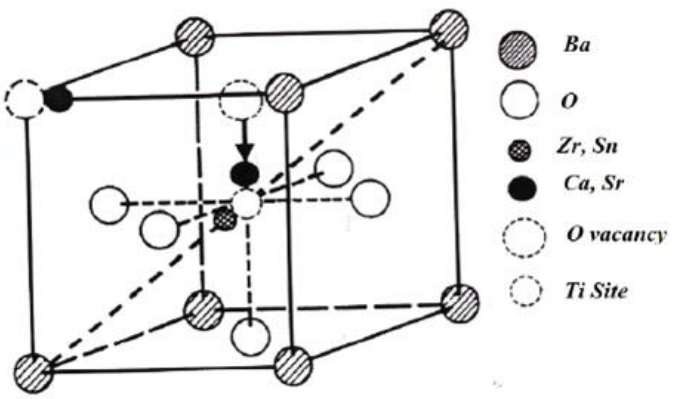

Figure 1.6: The cubic perovskite lattice of $BaTiO_3$ showing the location of various substituents.

In the ABO_3 oxides (figure 1.6), changing ions of different sizes, valences, and polarizabilities at both the A and B lattice positions yields dipolar defects and can present satisfactorily high degree of disorder so as to break translational symmetry and set a stop to the formation of a long-range ordered state. In the extremely polarizable host lattice, the presence of a dipolar impurity on a site can induce dipoles within a correlation length of that site. The dipolar motion is estimated to be correlated within this correlation length, leading to the creation of polar nanodomains. The previous studies shows that such nanodomains have been stated in many ABO_3 relaxors at temperatures far-off the peak in ε′(T). Now the existence of polar nanodomains is agreed to be vital to the comprehension of the properties of relaxors.

1.9.2 Relaxor vs. Normal Ferroelectric

The macroscopic properties of relaxor ferroelectrics are quantitatively dissimilar from proper ferroelectrics. Relaxor ferroelectrics differ from ordinary ferroelectrics in terms of their frequency and temperature dependent dielectric response. In order to appreciate and recognize the properties of relaxors, it is functional to relate some of their properties with those of normal ferroelectric. We can do so with a support of table 1.1 and figure 1.7.

Table 1.1: Relation between normal and relaxor ferroelectrics.

Property	Normal Ferroelectric	Relaxor Ferroelectric
Temperature Dependence of Dielectric Constant ε′(T)	Sharp 1st & 2nd order Transition about Curie Temperature T_C	Diffuse Transition about Curie Maximum T'_m
Frequency Dependence of Dielectric Constant ε′(f)	Weak	Strong
ε′(T) Behavior in Paraelectric Regime	Obeys Curie-Weiss Law $\frac{1}{\varepsilon'} = \frac{T - T_{CW}}{C}$	Obeys Modified Curie-Weiss Law $\frac{1}{\varepsilon'} = \frac{1}{\varepsilon'_m} + \frac{(T - T'_m)^{\gamma}}{C_1}$
Remanent Polarization	Large	Small
Scattering of Light	Strong Anisotropy (Birefringence)	Very Weak Anisotropy (Pseudo Cubic)
X-ray Diffraction	Line splitting below the structural phase transition	No X-ray line splitting due to pseudo cubic structure

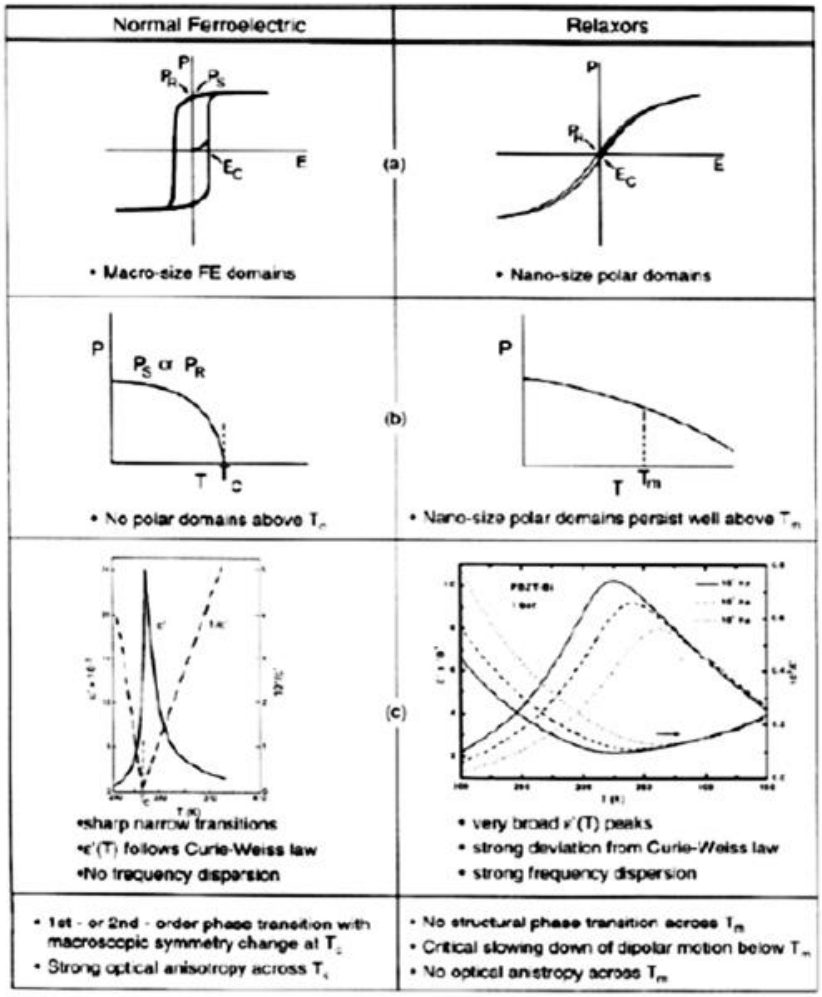

Figure 1.7: Contrast between the properties of normal ferroelectrics and relaxor ferroelectrics.

1.10 Theories of Relaxor Ferroelectric

To investigate the general properties of phase transitions, Ferroelectrics is a convenient system. Normal ferroelectrics experience a sharp phase transition at the Curie temperature. Above T_C, each atom within the unit cell is positioned on a high symmetry position causing no net dipole moment. To illustrate the relaxor properties many physical models such as order-disorder model, superparaelectric model, microdomain and macrodomain switching model, dipolar glass model and quenched random field model have been suggested by various researchers [29].

The first model was presented by Smolenskii and Isupov. They launched an idea of the "diffuse phase transition" causing from compositional fluctuations on a microscopic level [25]. According to this model the random distribution of ions on the B-site of the

$Pb(B'B'')O_3$ structure results the inhomogeneous chemical micro-regions with various compositions. The phase transition into the polar state (ferroelectric) takes place into distinct microregions, independent of each other, hence dissimilar Curie temperatures, which effects in a broad dielectric permittivity over a mean Curie temperature at approximately T'_m. In spite of this, the only structural atomic variation cannot define the frequency dispersion of $\varepsilon(T)$ in the locality of T_m.

Cross [7] extended Smolenskii's theory and proposed that relaxors may be considered a superparaelectric model by considering analogy between the polar microregions and the spin clusters in superparamagnets. He visualized relaxors as containing of small non-interacting polar-regions of various sizes with a local spontaneous polarization. The PNRs are able to switch between the equivalent orientations states according to the symmetry of the local polar phase. Thus the local polarization in each region can fluctuate under the thermal agitation and contribute to the orientation polarization. On cooling, the temperature and frequency dependence of dielectric permittivity is due to slowing down of the fluctuations of the local polarization vectors. The superparaelectric model successfully explains many of the features associated with relaxor ferroelectric behavior.

From both composition fluctuation model and superparaelectric theory, it becomes clear that nano-scale ordered micro-regions or clusters have a major role to play behind the relaxor ferroelectric behavior.

Later, Viehland et al [30], proposed a dipolar glass model and tried to explain the electric field dependence of the polarization in a vicinity of T_{max}. In this model relaxors were visualized as consisting of interacting Polar Regions in analogy of magnetic spin glasses. According to this model, the polarization fluctuations occurred above the static freezing temperature T_{VF} i.e. below T_{VF} the strength of the interactions between PNR's increases versus superparaelectric model [7] which does not consider these interactions into description.

The temperature dependence of the permittivity maximum was successfully modeled by the Vögel-Fulcher relationship. The Vögel-Fulcher law originally derived for the magnetic spin-glass systems is described as follows:

$$f = f_o \exp\left[-\frac{E_a}{k_B\left(T_m - T_{VF}\right)}\right] \qquad \textbf{1.4}$$

Where f_o is the pre-exponential factor, E_a is the activation energy, k_B is the Boltzmann constant, T'_m is the temperature corresponding to dielectric maxima and T_{VF} is the characteristic Vogel-Fulcher freezing temperature.

Bell [31] suggested a method to compute the dielectric properties of a superparaelectric material. He made use of the Landau–Ginzburg–Devonshire (LGD) theory of ferroelectrics by treating each polar cluster as a classical ferroelectric with a single phase transition temperature and that the volume of the polar clusters is a variable parameter. Hence, the relaxor ferroelectric behavior is illustrated by disorder with some clustering and freezing due the frustrated interactions between the clusters in the dipolar glass model.

1.11 Doped barium titanate ceramics

1.11.1 $BaZr_xTi_{1-x}O_3$ Ceramic

$BaZr_xTi_{1-x}O_3$ solid solution based on experimental data of dielectric study by several authors is shown in figure 1.8.

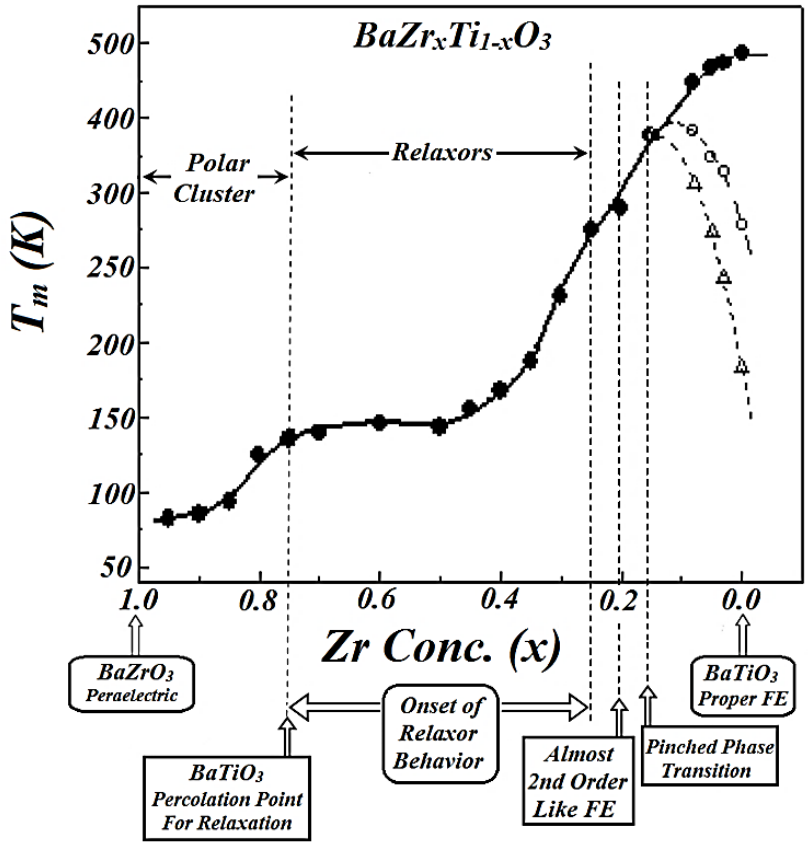

Figure 1.8: Phase diagram of *$BaZr_xTi_{1-x}O_3$* bulk ceramic.

The phase diagram clearly shows that with the addition of Zr^{+4} concentration, proper ferroelectric $BaTiO_3$ ($x = 0$) changes into a pinched phase transition at $x \sim 0.15$. The pinching effect of the phase transitions, results in a broadening of the dielectric maximum that can smooth the overall temperature response of permittivity.

In the composition range $0.15 < x < 0.25$, the system shows almost second order ferroelectric like diffuse phase transition behavior. The region showing relaxor behavior in $BaZr_xTi_{1-x}O_3$ system has been reported in the composition range $0.25 < x < 0.75$. Phase diagram show polar cluster like behavior for $x \geq 0.80$ from a simple dielectric i.e. pure $BaZrO_3$ *(x =1.00) [32, 33]*.

In summary Barium Zirconate Titanate ($BaZr_xTi_{1-x}O_3$) system depending on the composition, in succession describes the properties extending from simple dielectric (pure $BaZrO_3$) to polar cluster dielectric, relaxor ferroelectric, second order like diffuse phase transition, ferroelectric with pinched phase transitions and then to a proper ferroelectric (pure $BaTiO_3$). Up till now there has been no other single solid solution system that exhibits such a complex phase diagram.

1.11.2 $Ba_{1-x}Sr_xTiO_3$ Ceramic

BST is derived from the prototype $BaTiO_3$ (BTO) perovskites. BST undergoes phase transition at Curie temperature when it is in normal ferroelectric states. However, the Curie temperature depends upon the Ba/Sr ratio. The increase in amount of Sr in BTO shifts the Curie temperature and explicitly shows high dielectric constant around T_c than pure BTO. BST is purely in ferroelectric state and it has spontaneous polarization below T_c. the earlier study reveal that with addition of Sr^{2+} isovalant impurity in $BaTiO_3$ shows the relaxor features for $x \geq 0.12$ due to the permittivity maxima related with the cubic to tetragonal transition of BTO. A similar relaxor behavior has been reported at the Sr^{2+} rich ($x > 0.8$) end in $Ba_{1-x}Sr_xTiO_3$ system too. On addition of Sr, the variation of dielectric permittivity and Curie temperature gets broadened [34, 35].

It is reported by several researchers that room temperature $Ba_{1-x}Sr_xTiO_3$ exhibit cubic structure for compositions with 'x' ranging from 0.3 to 1 but from 0 to 0.3, it is found to be tetragonal [36-40]. The lattice parameters reported for ST and BT are ranging from 'a = 3.905 Å' to 'a = 3.994 Å' and 'c = 4.038 Å*'* [41].

1.12 Motivation

The motive to choose the $Ba_{1-x}Sr_xZr_{0.2}Ti_{0.8}O_3$ and $Ba_{1-x}Sr_xZr_{0.3}Ti_{0.7}O_3$ systems is to observe the relaxor behaviour in the system with strontium doping. As many researchers reported that BT ceramic exhibit relaxor properties when doped with Zr(*x*). The reported range of the concentration of Zr(*x*) upon which the normal ferroelectric transform into relaxor ferroelectric is $0.25 < x < 0.75$ in BT ceramic [31]. Similarly there is also reported that ferroelectric (normal) transform to relaxor ferroelectric upon doping of Sr(x) in BT ceramic. The reported range of Sr(x) substitution at which relaxor ferroelectric transformation occur is $x > 0.8$ but some researchers reported at $x < 0.8$ [35]. We wish to investigate whether the $Ba_{1-x}Sr_xZr_{0.2}Ti_{0.8}O_3$ (ferroelectric) system transform to relaxor ferroelectric with increasing Sr(x) concentration up to $x = 0.3$ or not. We assumed that this may occur since the smaller Sr ion may distort the lattice and thereby produce more and more frustration amongst the polar nano structures. We shall discover the effect (lattice parameter, XRD density, dielectric constant, Transition temperature) of Sr substitution in $Ba_{1-x}Sr_xZr_{0.2}Ti_{0.8}O_3$ the system.

In $Ba_{1-x}Sr_xZr_{0.3}Ti_{0.7}O_3$ system, we wish to effect on the relaxor properties in the nominal composition $BaZr_{0.3}Ti_{0.7}O_3$ system with increasing concentration of strontium upon doping. We wish to study that how diffusivity changes with increase in Sr and how the transition temperature varies with increase in Sr contents [42]. With various concentration of Sr, we wish to observe that how the dielectric constant modify with increasing concentration of Sr in the parent compound. We will fit the experimental data with different theoretical models and try to calculate the critical parameters (*Curie constant, Curie temperature, static freezing temperature T_{VF}, Activation energy etc.*) in order to find out the relaxor behavior [43].

Chapter 2 EXPERIMENTAL TECHNIQUES

This chapter designates experimental techniques used for characterizing the relaxor ferroelectric ceramic Sample in our research work. The precursors are mixed together by means of solid state route to form the desired phases. The X-Ray Diffractometer was used for investigation of the structure and confirmation of phases of all prepared samples. The dielectric data of all samples were measured by Wayne Kerr 4275 Meter Bridge.

2.1 Experimental Procedures

The overall experimental processes for bulk ceramics are summarized in figure 2.1.

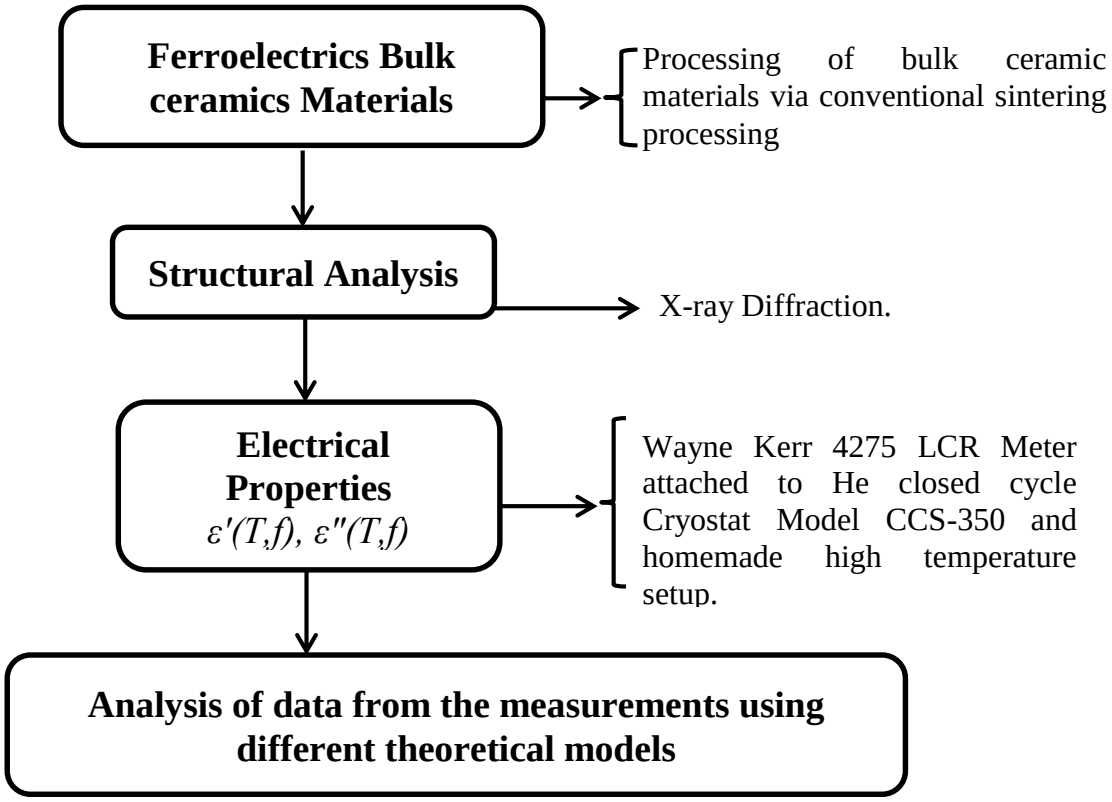

Figure 2.1: The overall experimental processes.

2.2 Fabrication of bulk ferroelectric materials

There are various method to prepare bulk materials but solid state reaction method is simplest and common to prepare bulk materials even if they are ferromagnetic, ferroelectric or multiferroic. In this method different type of non-volatile solids are mixed

together and then heated at high temperature to get the required bulk material. The steps which are required to produce a desired bulk material are shown in figure 2.2.

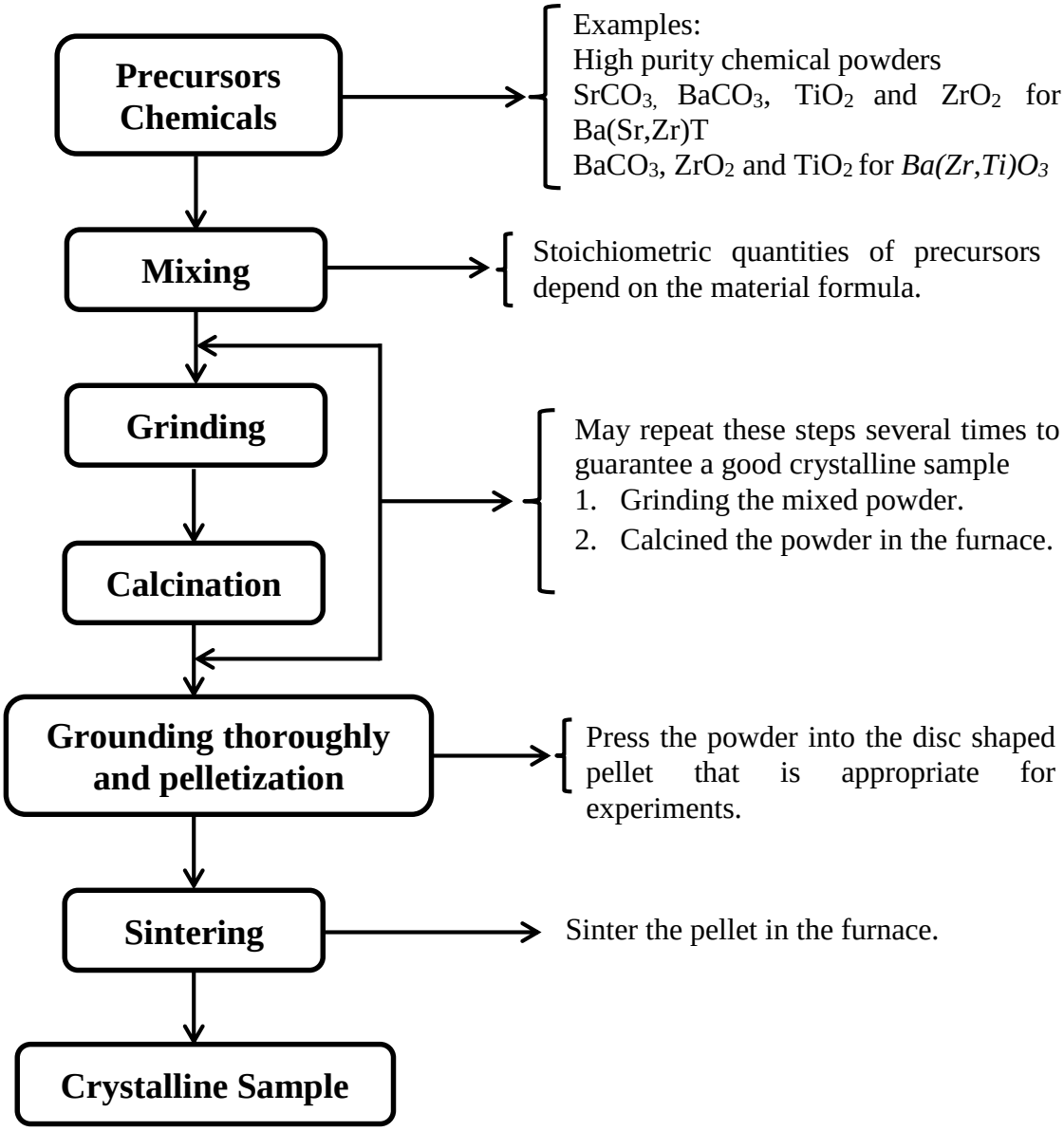

Figure 2.2: **Steps involve during fabrication of Bulk material.**

First of all take the appropriate stoichiometric ratio of all precursors, mixed and grind them together in pestle and mortar for almost 3 hours so that we can get uniform small particle size. The process of grinding may be repeated several times. The grinded material is then heated in furnace in an alumina or porcelain pot. Pots of porcelain and alumina separately used for the heat treatment and synthesis of the powders.

2.2.1 Furnace

We used box furnace for calcination of precursors at 1200 ºC and sintering at 1400 ºC of our Sample. The maximum operating temperature of the furnace is 1600 ºC. The furnace is controlled by digital programing installed in a furnace. The program can be set according to our desired conditions i.e. desired temperature for calcination/sintering, ramp rate, duration of stay at desired temperature, annealing rate. The furnace is capable of multiprogramming, for example we can choose multiple set points for our sample if required.

2.3 X-ray Diffractometer

The crystal structure of bulk samples was determined by reviewing the X-Ray diffraction pattern. The diffractometer used was a PANalytical Empyrean system with Prefix optical parts and stationary sample stage (figure 2.3). The functional voltage was 45 kV and the current was 40 mA. The basis of X-ray is copper (Cu) with characteristic X-rays with wavelengths $K\alpha_1$~ 1.540593 Å, $K\alpha_2$ ~ 1.54442 Å and $K\beta$ ~ 1.54187 Å. The most common uses of these X-rays are high resolution directions, quantitative analysis, phase identification and normal powder diffraction.

Figure 2.3: X-ray diffractometer

It is a great tool for characterizing the products of a solid state synthesis reaction by carrying out diffraction analysis of materials. At the simplest level, diffraction patterns can be examined for phase identification that is, determining what crystalline substances are existing in a particular sample. For the period of X-ray diffraction analysis, the atomic planes of a crystal cause an incident X-ray beams to interfere with one another as they leave the crystal. Because the X-ray beam has a specific wavelength, for any given *d* spacing (distance between adjacent atomic planes) there are only specific angles at which the exiting rays will be in phase and therefore, will be picked up by the detector producing a peak on the diffractogram. Each crystalline substance has a unique X-ray diffraction pattern. Each crystalline particle (or grain) has a large number of unit cells.

2.3.1 Essential Parts of Diffractometer

- **X-ray Tube:** the source of X-rays.
- **Incident Beam Optics**: it allows only the suitable X-ray beam before it interacts with the sample.
- **The Goniometer:** it is used for mounting the sample and detector in such a way that condition for X-ray diffraction obeyed.
- **Sample Holder:** it is a device which holds the sample to be analyzed.
- **Receiving Side Optics:** it is used after the interaction of X-ray beam with the sample.
- **Detector:** it counts the number of x-rays scattered by the sample and it moves in a circle according to given step angle.

2.3.2 Diffractometer working principle for Powder sample

The polycrystalline sample is exposed to the incident beam of X-rays such that the Bragg's condition for diffraction is obeyed. The sample composed of fine and arbitrarily oriented particles, each crystalline grain (particle) have large number of unit cells oriented randomly which ensure that some of the particles are oriented in such a way that the possible set of planes are presented by the sample to incident X-ray beam. After the interaction between X-ray beam and specimen the reflected X-ray beam is recorded at the detector which is situated at the opposite side to the X-ray tube. A recorder automatically plot intensity as a function of 2θ of diffracted beam.

A set of fixed divergence slits are provided with the apparatus. These slits are marked as 4º, 2º, 1º, 1/2º and 1/4º and are used for the polycrystalline sample phase analysis. The Bragg-Brentano geometry as shown in figure 2.4 is used for the analysis of flat polycrystalline materials.

In Bragg-Brentano para-focusing geometry, the incident X-ray beam from the line focus of the X-ray tube diverges in the diffraction plane until it irradiates the sample. The diffracted X-ray beam converges from the sample until it passes through the receiving slit before diverging again.

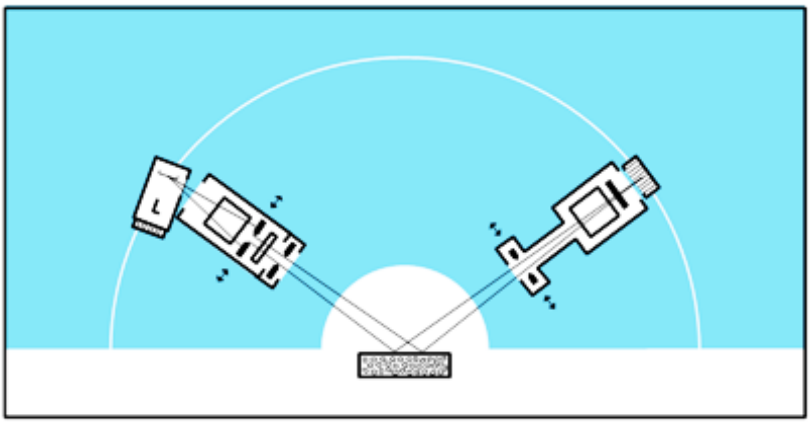

Figure 2.4: Powder sample configuration for XRD measurements.

For normal powder diffraction, a fixed divergence slit (1º) is used to control the divergence of the incident beam. Receiving slits (1/16º) are placed in the focusing point of the diffracted X-ray beam. The opening of the slit controls the resolution of the scan.

2.4 Dielectric Properties Measurement

The dielectric properties were measured by LCR meter. Dielectric constant was determined from capacitance measurements made in the frequency range 0.2-500 *kHz* at different temperatures. The LCR meter used was the Wayne-Kerr model 4275 (figure 2.5).

Figure 2.5: LCR meter

The LCR meter records the capacitance and dissipation factor simultaneously. The sample was cooled down in a closed cycle helium cryostat and temperature controller was there for controlling the heating and cooling rate of the sample. The block diagram for complete setup of dielectric measurement is shown below in figure 2.6.

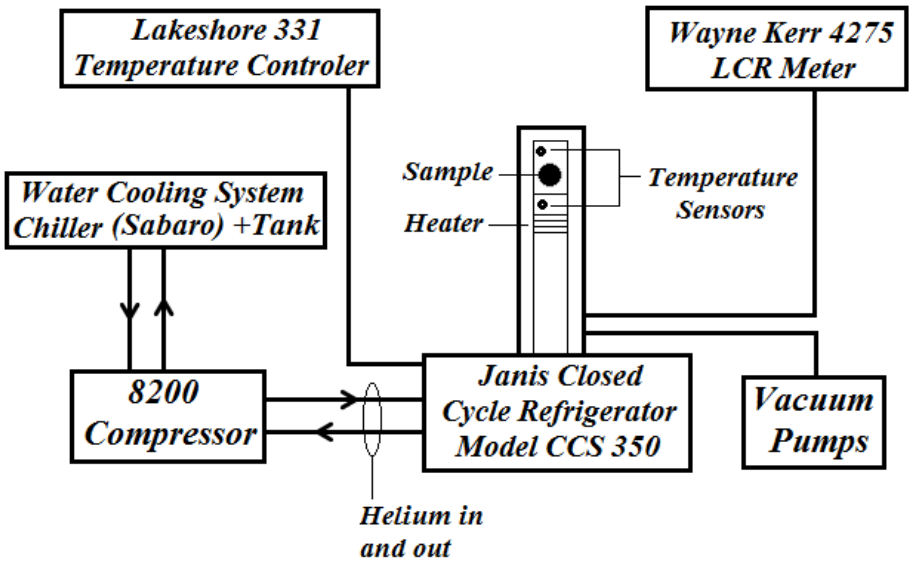

Figure 2.6: Schematic block diagram of the dielectric measurement setup.

2.4.1 Cryostat

Janis closed cycle refrigerator (CCR) system model CCS-350 was used for the dielectric constant measurements. The schematic diagram of the complete system is shown figure 2.7. The main parts of the Janis CCR system includes

- Compressor (Model 8200)
- Cold Head
- Gas Lines

- Vacuum Jacket
- Radiation Shield
- Temperature controller (331 LakeShore)

CCR system operates in the temperature range 10 K to 325 K and requires no liquid helium. Helium gas is compressed and expanded based on Gifford-McMahon (M-G) thermodynamic cycle using compressor (Model 8200) in a closed loop. During the expansion phase of each cycle, heat is removed from the cold finger on which sample is mounted. A TG-120-CU GaAlAs diode temperature controller and a 25 ohm heater are installed on the cold finger to measure and control the temperature precisely. Prior to cool down, the shroud is evacuated up to 1.0×10^{-4} torr using diffusion pump. Better vacuum level provides greater insulation, resulting in shorter cool down times and lower final temperatures.

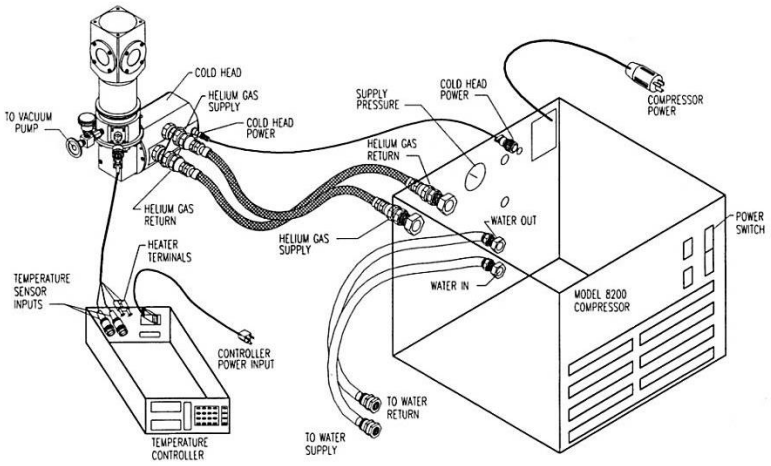

Figure 2.7: Complete view of setup used for dielectric constant measurements.

2.4.2 Sample Holder

Sample was attached on the sample holder made of brass with dimension of $16\ mm\times 30\ mm\times 4mm$ and attached at top end of cold finger as shown in figure 2.8. Mica sheet is attached on the brass sample holder which offers the better thermal contact between sample and sample holder while shielding it electrically. Typical size of the sample used to measure dielectric constant is circular pellet of diameter 10-12 mm. Two copper leads were attached on the sample using silver paint. An additional TG-120-CU GaAlAs diode thermometer is attached on the sample holder close to the sample for accurate measurement of the sample temperature.

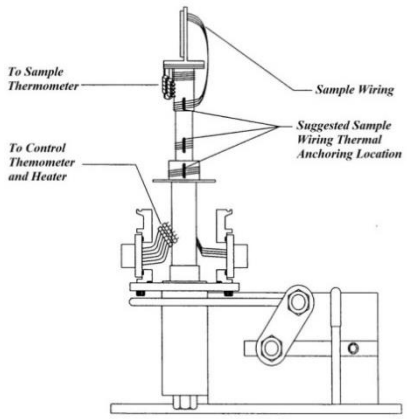

Figure 2.8: **System wiring inside closed cycle system model CCS-350.**

2.4.3 Temperature Controller (331 LakeShore)

The temperature controller model 331 of Lake Shore was used to control and measure the temperature of the closed cycle refrigerator and the sample. Model 331 temperature controller has two sensor inputs with maximum heater output of 50 W for sensor-A and 1 W for sensor-B. A TG-120-CU GaAlAs diode thermometer and 25 ohm control heater attached at cold finger of closed cycle system were connected with input of sensor-A and were used to control and measure the temperature of cryostat while sensor attached on sample holder was contacted at input of sensor-B and was used to measure the temperature of sample.

2.4.4 Dielectric Constant

The ratio of displacement vector **D** to the electric field intensity **E** is defined as dielectric constant ε. It is some time called relative permittivity and quantitivly it measures the degree to which a medium can resist flow of charges in material capacitance

$$\boldsymbol{\varepsilon = \frac{D}{E}} \qquad \textbf{2.1}$$

The material which has a high dielectric constant will have larger capacity to store charges and so concluded that it has high capacitance too.

To understand the behaviour of dielectric, we have to consider a parallel plate capacitor. Ain order to form parallel plate capacitor, two conducting plates having area "A" separated by a distance "d" without any dielectric introduced in between the two plates. The schematic diagram is shown in figure 2.9. Let connect the plates of the capacitor with the terminals of a battery, having potential difference V across its terminals, a charge Q

will deposit on plates. The upper plate is negatively charged while the lower plate is positively charged.

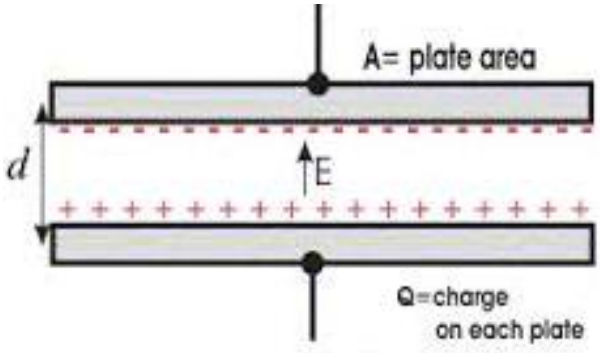

Figure 2.9: **Parallel Plate Capacitor**

In such a case, the electric field between the plates is the sum electric field due to individual plates.

$$E_o = E_1 + E_2$$

$$E_o = (\sigma/2\varepsilon_0) + (\sigma/2\varepsilon_0)$$

Thus, $$E_o = \sigma/\varepsilon_0 \quad \textbf{2.2}$$

The electric field in the region between the plates of parallel plate capacitor is thus given by $E = \sigma/\varepsilon_0$. If the potential difference between the plates of capacitor is then

$$V = E_o d \quad \textbf{2.3}$$

Therefore,

$$V = (\sigma/\varepsilon_0)d \quad \textbf{2.4}$$

We substitute σ with Q/A in the last equation, hence

$$V = (Q\ d)/(A\ \varepsilon_0)$$

Reshuffling the above equation gives

$$Q/V = (\varepsilon_0 A)/d$$

But Q/V is the capacitance.i.e. $$C_o = (\varepsilon_0 A)/d \quad \textbf{2.5}$$

Let inspect what occurs if the space between the two plates is filled with a dielectric material of permittivity ε. If a dielectric is positioned between the plates of a capacitor the capacitance of the capacitor increases, such that

$$C = \varepsilon C_o$$

$$C = \varepsilon_r (\varepsilon_0 A)/d$$

$$\varepsilon_r = Cd/\varepsilon_0 A \quad \textbf{2.6}$$

The product $\varepsilon_r\varepsilon_o = \varepsilon$ is the called permittivity of the dielectric.

2.4.5 Dielectric Loss

The electric flux density with the alternating fields of a parallel plate capacitor filled with a materials characterized by ε can be stated as

$$D(t) = \mathrm{Re}\left[\varepsilon_o \varepsilon_r E_o \exp(i\omega t)\right] \quad \textbf{2.7}$$

Here the electric flux density is time varying quantity, so there will be a flow of current and the current density will be

$$J(t) = \frac{d(D)}{dt} = \mathrm{Re}\left[\varepsilon_o \varepsilon_r \cdot i\omega E_o \exp(i\omega t)\right] \quad \textbf{2.8}$$

Since ε_r is a complex quantity, we can write,

$$J(t) = \omega \varepsilon_o E_o \,\mathrm{Re}\left[i(\varepsilon' - i\varepsilon'')(\cos\omega t + i\sin\omega t)\right]$$

$$J(t) = \omega\, \varepsilon_o E_o(\varepsilon'' \cos\omega t - \varepsilon' \sin\omega t) \quad \textbf{2.9}$$

To derive a circuit analogue of the phenomenon of dielectric losses a parallel plate capacitor with unit area of cross-section of the plates and separated by unit length. If the applied voltage is, $E_o cos\omega t$ then from Eq. 2.9, which shows that, the dielectric may be considered to be made up of a *parallel* combination of resistance and capacitance. If R is the resistance and C is the capacitance of the dielectric,

$$J(t) = \frac{E_o \cos\omega t}{R} - E_o \omega C \sin\omega t$$

With $R = 1/\omega\varepsilon_o\varepsilon''$ and $C = \varepsilon_o\varepsilon'$ with the general expression of capacitance as ($A = 1\ m^2$ and $d = 1\ m$)

$$C = \frac{\varepsilon'\varepsilon_o A}{d} \quad \textbf{2.10}$$

As $\varepsilon'' \rightarrow 0$ and $R \rightarrow \infty$.The loss $\tan\delta$ is defined as $\varepsilon''/\varepsilon'$ and is the measure of the dielectric losses is

$$\tan\delta = \frac{\varepsilon''}{\varepsilon'} = \frac{1}{\omega RC} \quad \textbf{2.11}$$

Where $\omega = 2\pi f$ is the applied frequency (in Hertz (Hz)), R and C are the corresponding resistance (in Ohms (Ω)) and capacitance (in Farads (F)) respectively.

Chapter 3 SYNTHESIS AND STRUCTURAL CHARACTERIZATION

In this chapter we are going to describe the method used to synthesize the various relaxor ferroelectrics and Non-Relaxor ferroelectrics ceramics in this research work. The solid state reaction route was used to synthesize the ceramic compositions with general formula $Ba_{1-x}Sr_xZr_yTi_{1-y}O_3$ (y = 0.2 and x =0, 0.1, 0.2, 0.3, with y =0.3 and x =*0, 0.1, 0.2, 0.24, 0.28, 0.3*) and X-ray Diffractometer was used for the structural analysis of the Synthesized Compositions.

3.1 Solid State Reaction Route

Solid state reaction route is the most traditional and broadly used method for the synthesis of polycrystalline materials from a combination of starting solid materials. Main steps for synthesis by solid state reaction involve calcination and sintering. Heat treatment is executed at 70% of melting point of material used. Precursors are mixed and grinded thoroughly for the homogenization of required phase.

3.1.1 Chemicals

Ceramic bulk samples of different compositions $Ba_{1-x}Sr_xZr_yTi_{1-y}O_3$ fabricated using solid state reaction methods. Carbonates and oxide powders (table 3.1) were mixed and the relative amounts were determined by stoichiometry. All these oxide powders were having more than 99% purity.

Table 3.1: Component oxides and carbonates used in this study.

Precursors	**Formula**	**Purity (%)**	**Molecular Weight**	**Supplier**
Barium Carbonate	$BaCO_3$	99	197.3359	Avonchem
Strontium Carbonate	$SrCO_3$	99	147.6289	Cerac
Titanium Oxide	TiO_2	99-100	79.8658	Riedel-de Haën
Zirconium Oxide	ZrO_2	99	123.2228	Fluka

3.1.2 Weighing of Precursors and Chemical Reaction

The chemical reaction for general formula for perovskite ABO_3 with co-doping at **A (Sr**) and **B (Zr)** site in Barium titanate having perovskite structure is

$$(1-x)BaCO_3 + xSrCO_3 + (1-y)TiO_2 + yZrO_2 \rightarrow Ba_{1-x}Sr_xZr_yTi_{1-y}O_3 + CO_2 \quad \textbf{(3.1)}$$

All the chemicals at left sides in above chemical equation are raw materials and there at the right side of the equation we get a desired solid material with carbon dioxide gas.

a) $Ba_{1-x}Sr_xZr_{0.2}Ti_{0.8}O_3$ (y= 0.2)

Stoichiometric composition of $Ba_{1-x}Sr_xZr_{0.2}Ti_{0.8}O_3$ ceramics with x = 0, 0.10, 0.20, 0.24, 0.28 and 0.3 were prepared by thoroughly mixing the stoichiometrically weighed oxides and carbonates powders. The samples prepared are as follow;

The general chemical reaction of $Ba_{1-x}Sr_xZr_{0.2}Ti_{0.8}O_3$ is written as below

$(1-x)BaCO_3 + xSrCO_3 + 0.8TiO_2 + 0.2ZrO_2 \rightarrow Ba_{1-x}Sr_xZr_{0.2}Ti_{0.8}O_3 + CO_2$

- ***$BaZr_{0.2}Ti_{0.8}O_3$***

For *x= 0,* chemical formula is

$$BaCO_3 + 0.8TiO_2 + 0.2ZrO_2 \rightarrow BaZr_{0.2}Ti_{0.8}O_3 + CO_2$$

The ratio of molecular weight of precursors are

$BaCO_3$	:	$SrCO_3$	:	TiO_2	:	ZrO_2
197.335	:	0	:	63.89264	:	24.64456
4.9334	:	0	:	1.5973	:	0.6161

Typical mass of the sample is 6.0466 gms

- ***$Ba_{0.9}Sr_{0.1}Zr_{0.2}Ti_{0.8}O_3$***

For x = 0.1, chemical formula is

$$0.9BaCO_3 + 0.1SrCO_3 + 0.8TiO_2 + 0.2ZrO_2 \rightarrow Ba_{0.9}Sr_{0.1}Zr_{0.2}Ti_{0.8}O_3 + CO_2$$

The ratio of molecular weight of precursors are

$BaCO_3$	:	$SrCO_3$	:	TiO_2	:	ZrO_2
177.60231	:	14.76289	:	63.89264	:	24.64456
4.44	:	0.3690	:	1.5973	:	0.6161

Typical mass of sample is 5.9222 gms

- ***$Ba_{0.8}Sr_{0.2}Zr_{0.2}Ti_{0.8}O_3$***

For *x= 0.2,* chemical formula is

$$0.8BaCO_3 + 0.2SrCO_3 + 0.8TiO_2 + 0.2ZrO_2 \rightarrow Ba_{0.8}Sr_{0.2}Zr_{0.2}Ti_{0.8}O_3 + CO_2$$

The ratio of molecular weight of precursors are

$BaCO_3$	:	$SrCO_3$	:	TiO_2	:	ZrO_2
157.86848	:	29.52578	:	63.89264	:	24.64456
3.9467	:	0.7381	:	1.5973	:	0.6161

Typical mass of sample is 5.798 gms

- ***$Ba_{0.7}Sr_{0.3}Zr_{0.2}Ti_{0.8}O_3$***

For *x= 0.3*, chemical formula is

$$0.7BaCO_3 + 0.3SrCO_3 + 0.8TiO_2 + 0.2ZrO_2 \rightarrow Ba_{0.7}Sr_{0.3}Zr_{0.2}Ti_{0.8}O_3 + CO_2$$

The ratio of molecular weight of precursors are

$BaCO_3$	:	$SrCO_3$	:	TiO_2	:	ZrO_2
138.13513	:	44.28867	:	63.89264	:	24.64456
3.4534	:	1.10722	:	1.5973	:	0.6161

Typical mass of sample is 5.67382 gms

b) $Ba_{1-x}Sr_xZr_{0.3}Ti_{0.7}O_3$ (y= 0.3)

Stoichiometric composition of $Ba_{1-x}Sr_xZr_{0.2}Ti_{0.8}O_3$ ceramics with x =0, 0.10, 0.20, 0.24, 0.27 and 0.3 were prepared by thoroughly mixing the stoichiometrically weighed oxides and carbonates powders. The samples prepared are as follow;

The general chemical reaction of $Ba_{1-x}Sr_xZr_{0.3}Ti_{0.7}O_3$ is written as below.

$$(1-x)BaCO_3 + xSrCO_3 + 0.7TiO_2 + 0.3ZrO_2 \rightarrow Ba_{1-x}Sr_xZr_{0.3}Ti_{0.7}O_3 + CO_2$$

- ***$BaZr_{0.3}Ti_{0.7}O_3$***

For *x= 0*, chemical formula is

$$BaCO_3 + 0.7TiO_2 + 0.3ZrO_2 \rightarrow BaZr_{0.3}Ti_{0.7}O_3 + CO_2$$

The ratio of molecular weight of precursors are

$BaCO_3$	:	$SrCO_3$	:	TiO_2	:	ZrO_2
197.3359	:	0	:	55.90606	:	36.96684
4.9334	:	0	:	1.3976	:	0.9241

Typical mass of sample is 6.1549 gms

- ***$Ba_{0.9}Sr_{0.1}Zr_{0.3}Ti_{0.7}O_3$***

For *x= 0.1*, chemical formula is

$$0.9BaCO_3 + 0.1\ SrCO_3 + 0.7TiO_2 + 0.3ZrO_2 \rightarrow Ba_{0.9}Sr_{0.1}Zr_{0.3}Ti_{0.7}O_3 + CO_2$$

The ratio of molecular weight of precursors are

$BaCO_3$	:	$SrCO_3$	:	TiO_2	:	ZrO_2
177.60231	:	14.76289	:	55.90606	:	36.96684
4.44	:	0.3690	:	1.3976	:	0.9241

Typical mass of sample is 6.0305 gms

- ***$Ba_{0.8}Sr_{0.2}Zr_{0.3}Ti_{0.7}O_3$***

For *x= 0.2*, chemical formula is

$$0.8BaCO_3 + 0.2\ SrCO_3 + 0.7TiO_2 + 0.3ZrO_2 \rightarrow Ba_{0.8}Sr_{0.2}Zr_{0.3}Ti_{0.7}O_3 + CO_2$$

The ratio of molecular weight of precursors are

$BaCO_3$	:	$SrCO_3$	:	TiO_2	:	ZrO_2
157.86872	:	29.52578	:	55.90606	:	36.96684
3.9467	:	0.7381	:	1.3976	:	0.9241

Typical mass of sample is 5.9063 gms

- ***$Ba_{0.76}Sr_{0.26}Zr_{0.3}Ti_{0.7}O_3$***

For *x= 0.24*, chemical formula is

$$0.76BaCO_3 + 0.24\ SrCO_3 + 0.7TiO_2 + 0.3ZrO_2 \rightarrow Ba_{0.76}Sr_{0.24}Zr_{0.3}Ti_{0.7}O_3 + CO_2$$

The ratio of molecular weight of precursors are

$BaCO_3$	:	$SrCO_3$	:	TiO_2	:	ZrO_2
149.97528	:	35.43094	:	55.90606	:	36.96684
3.7494	:	0.8858	:	1.3976	:	0.9241

Typical mass of sample is 5.8567 gms

- ***$Ba_{0.73}Sr_{0.27}Zr_{0.3}Ti_{0.7}O_3$***

For *x=0.27*, chemical formula is

$$0.73BaCO_3 + 0.27SrCO_3 + 0.7TiO_2 + 0.3ZrO_2 \rightarrow Ba_{0.73}Sr_{0.27}Zr_{0.3}Ti_{0.7}O_3 + CO_2$$

The ratio of molecular weight of precursors are

$BaCO_3$	:	$SrCO_3$	:	TiO_2	:	ZrO_2
144.05521	:	39.8598	:	55.90606	:	36.96684
3.6014	:	0.9965	:	1.3976	:	0.9241

Typical mass of sample is 5.8194 gms

- $Ba_{0.7}Sr_{0.3}Zr_{0.3}Ti_{0.7}O_3$

For $x = 0.3$, chemical formula is

$$0.7BaCO_3 + 0.3\,SrCO_3 + 0.7TiO_2 + 0.3ZrO_2 \rightarrow Ba_{0.7}Sr_{0.3}Zr_{0.3}Ti_{0.7}O_3 + CO_2$$

The ratio of molecular weight of precursors are

$BaCO_3$	:	$SrCO_3$	:	TiO_2	:	ZrO_2
138.13513	:	44.28867	:	55.90606	:	36.96684
3.4534	:	1.1072	:	1.3976	:	0.9241

Typical mass of sample is 5.7821 gms

3.1.3 Mixing and Grinding

The prerequisite amounts of raw materials were thoroughly assorted in an agate mortar with appropriate amount of acetone (volatile organic liquid) for 2 to 3 hr. The volatile organic liquid was added in the assortment for homogenization of required phases.

3.1.4 Calcination

After required and proper mixing, desired compositions listed above, were calcined at 1200 ºC for 2 hours inside a box furnace at heating and cooling rate 5 ºC /min where the compositions are kept in porcelain crucible. The calcined powders were reground to a fine powder so that all agglomerates should break by an agate mortar and pistel.

3.1.5 Pellets formation

After calcination, the reground powders were pressed into pellets under a uniaxial pressure of 5 ton for 10 minutes. Before powders were pressed into pellets PVA (Polyvinayl

Alchohol) is added at 5 wt% to the powders and was used as a binder to improve the green strength of powder compacts.

3.1.6 Sintering

The pellets of compositions $Ba_{1-x}Sr_xZr_{0.2}Ti_{0.8}O_3$ *and* $Ba_{1-x}Sr_xZr_{0.3}Ti_{0.7}O_3$ $(0 \leq x \leq 0.3)$ were taken on a magnesia plate and sintered at 1400 ºC for 4 hours in a programmable box furnace at heating rate of 10 ºC/min (Figure 3.1). During the sintering process the added binder was burnout at 500–600 ºC. The pelletize form of the powder after sintering is strong, dense, closely packed grain and randomly oriented crystallographic planes which is vital for electrical measurement. The temperature of calcination is always less than the sintering temperature.

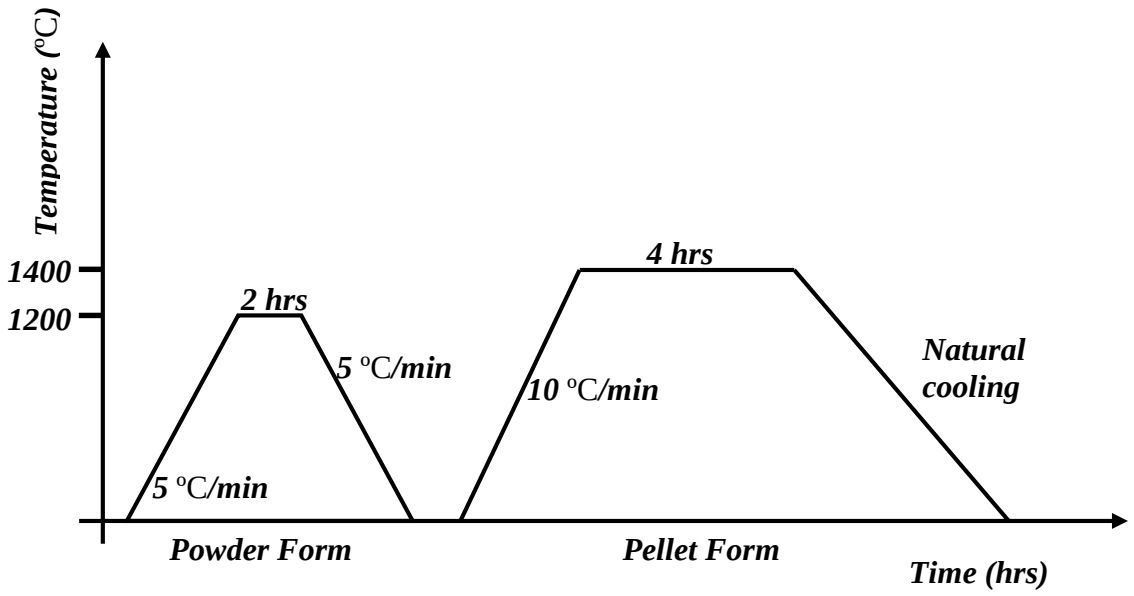

Figure 3.1: The overall heat treatment of the BSZT compositions.

3.2 Structural Characterization

In order to calculate the structure of atomic lattice, interplanar spacing should be comparable to wavelength of radiation used. X-rays have wavelength similar to the size of atoms, they are useful to explore with in crystals. The atoms in a crystal are arranged in a regular pattern, and in a very few directions we will have constructive interference. The waves will be in phase and there will be well defined X-ray beams leaving the sample at various directions. Hence, a diffracted beam may be described as a beam composed of a large number of scattered rays mutually reinforcing one another.

The constructive and destructive interference of coherently scattering radiations is controlled by geometry at the interatomic level and is governed by well-known Bragg's law

$$n\lambda = 2d\sin\theta \quad \textbf{3.2}$$

Where θ is the Bragg's angle, λ is the wavelength of the X-rays and d is the interplanar spacing. The interplanar spacing for the *hkl* plane of a cubic and systems are:

$$\frac{1}{d^2_{hkl}} = \frac{h^2 + k^2 + l^2}{a^2} \quad \textbf{3.3}$$

Where *h*, *k* and *l* are the Miller indices of the planes of atoms. Bragg's condition requires that a suitable combination of λ and θ be found for efficient reflection.

Powder X-ray diffraction (XRD) measurements were performed at room temperature over the range 2θ = 20−80° with a *PANalytical Empyrean* diffractometer using Cu Kα radiation (λ = 1.5406 Å). The data is taken as a continuous scan type having step size of 0.02˚ degree and step time of three seconds.

3.2.1 Crystal structure analysis of Ba1-xSrxZr0.2Ti0.8

The room temperature X-ray diffraction spectra of sintered Sr doped barium zirconium titanate ($Ba_{1-x}Sr_xZr_{0.2}Ti_{0.8}$) samples are shown in Figure 3.2. All the samples were found to be single phase, with no additional phase and polycrystalline with no preferred orientation. The peaks in the XRD patterns can all be indexed and correspond to a cubic perovskite structure. The patterns are in good agreement with the standard card PCPDF # 36001 and PCPDF # 00-001-1018.

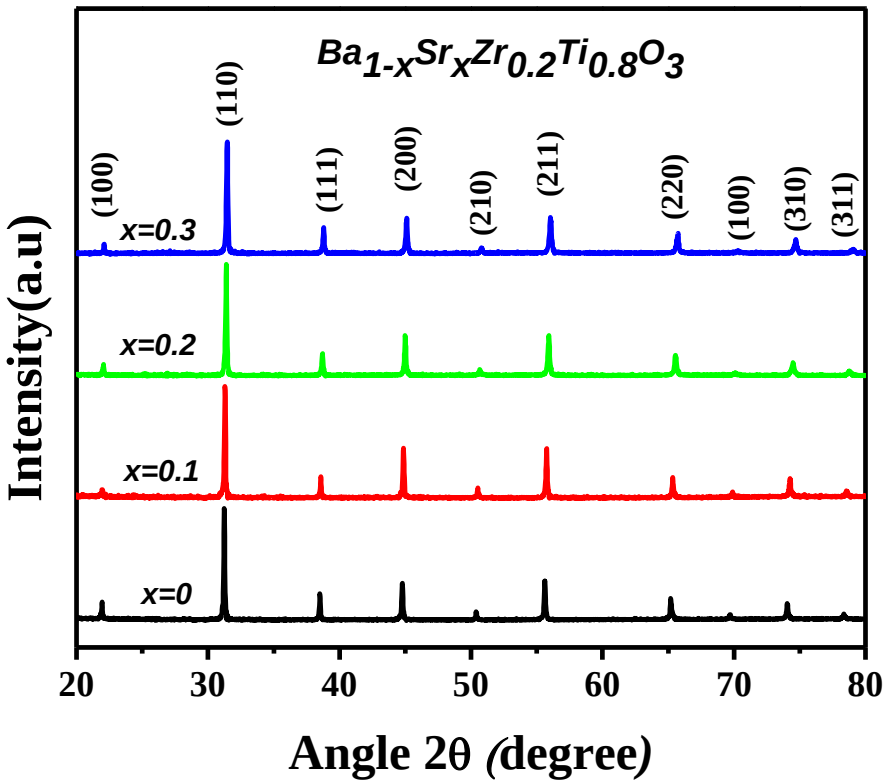

Figure 3.2: Xrd Pattern of the composition $Ba_{1-x}Sr_xZr_{0.2}Ti_{0.8}O_3$.

It is observed form the XRD-pattern that the principal diffraction peak shift toward the higher angle with increasing of Sr content (Figure 3.3). This shift is due to the incorporation of smaller ionic radii Sr^{2+} (1.18 Å) in place of larger ionic radii Ba^{2+} (1.37 Å). The strains developed due to the difference on size of Sr^{2+} and Ba^{2+} cations. This is clear indication that the Sr is systematically dissolved in the $Ba\,Zr_{0.2}\,Ti_{0.8}\,O_3$ lattice in the studied compositions. No splitting of (200) peak is observed which reveal that the structure is cubic perovskite.

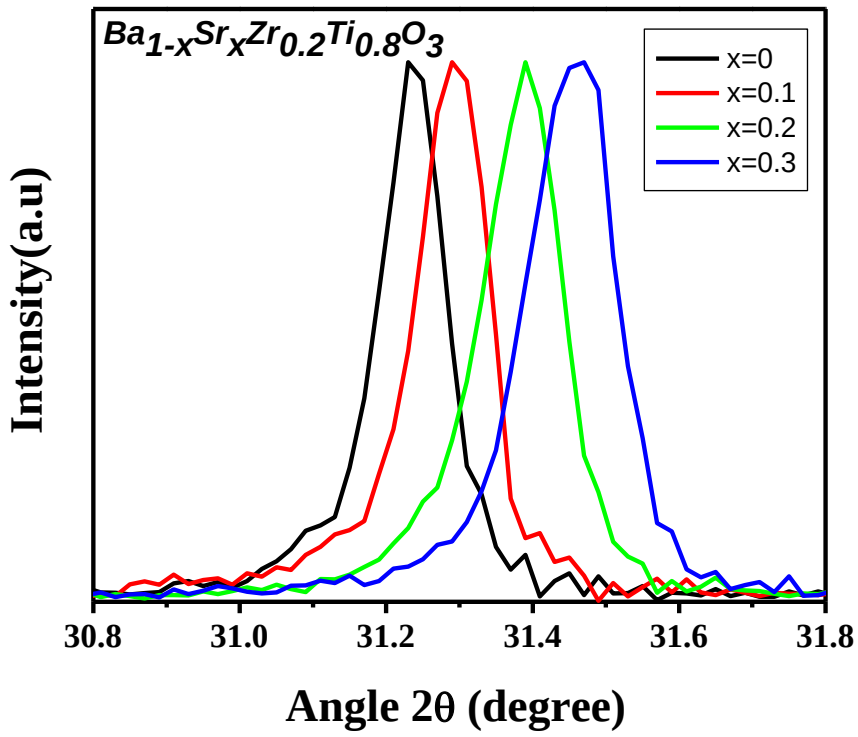

Figure 3.3: XRD peak variation of composition $Ba_{1-x}Sr_xZr_{0.2}Ti_{0.8}O_3$

The lattice constant of the sample was determined by the Eq. 3.3 and are listed in Table 3.2. This data show a decrease in the lattice constant with increase in Sr content in the samples, the lattice is contract due to the smaller size of Sr ion. Figure 3.4 shows the graphical representation of the data in table 3.2.

Table 3.2: Values of the lattice parameter of $Ba_{1-x}Sr_xZr_{0.2}Ti_{0.8}O_3$ calculated from the XRD diffractogram.

x	$Ba_{1-x}Sr_xZr_{0.2}Ti_{0.8}O_3$	Lattice Parameter (Å)
0	$Ba\ Zr_{0.2}\ Ti_{0.8}\ O_3$	4.044 ± 0.002
0.1	$Ba_{0.9}\ Sr_{0.1}Zr_{0.2}\ Ti_{0.8}\ O_3$	4.035 ± 0.001
0.2	$Ba_{0.8}Sr_{0.2}\ Zr_{0.2}\ Ti_{0.8}\ O_3$	4.024 ± 0.001
0.3	$Ba_{0.7}Sr_{0.3}Zr_{0.2}\ Ti_{0.8}\ O_3$	4.014 ± 0.002

The X-ray density or theoretical density was estimated using the relation

$$\rho_{XRD} = \frac{M}{N_A.a^3} \qquad \textbf{3.4}$$

Where *M* is the molecular weight of the particular perovskite, a^3 is the volume of the cubic unit cell and *N* is the Avogadro's number. The variation in ρ_{XRD} as function of *Sr* concentration is shown in figure 3.4. From figure 3.4 it is observed that the ρ_{XRD} decreases with the addition of Sr^{+2} ion content, which is also attributed to the ionic radii of constituent ions causing decrease in lattice parameter.

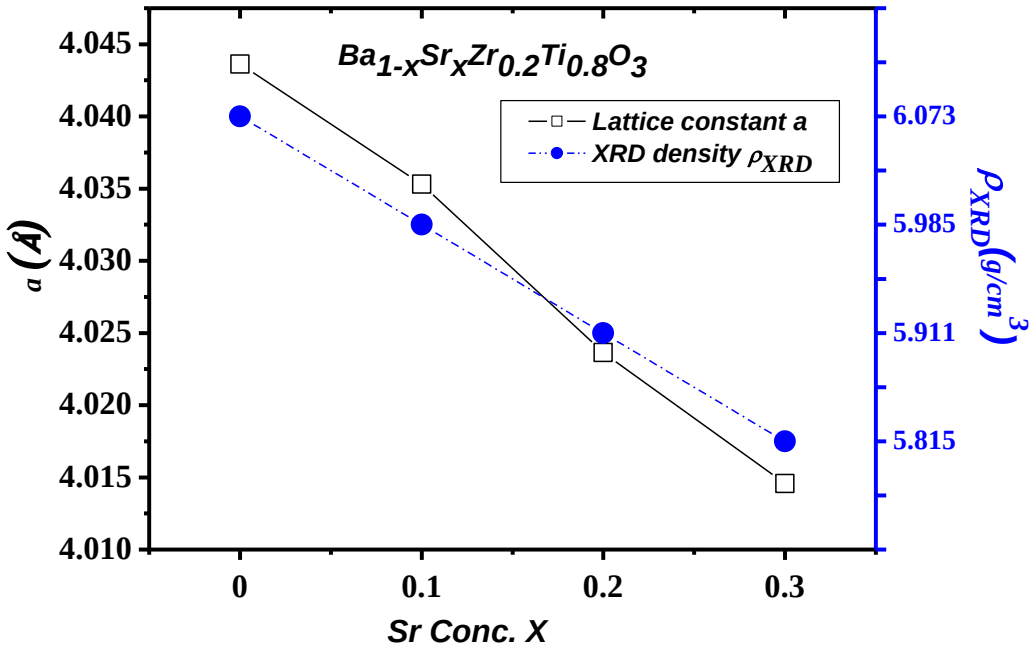

Figure 3.4: Lattice parameter and ρ_{XRD} variation of composition $Ba_{1-x}Sr_xZr_{0.2}Ti_{0.8}O_3$

3.2.2 Crystal structure analysis of $Ba_{1-x}Sr_xZr_{0.3}Ti_{0.7}O_3$

The room temperature X-ray diffraction spectra of sintered Sr doped barium zirconium titanate ($Ba_{1-x}Sr_xZr_{0.3}Ti_{0.7}O_3$) samples are shown in **Error! Reference source ot found.**. All the samples were found to be single phase, with no additional phase and polycrystalline with no preferred orientation. The peaks in the XRD patterns can all be indexed and correspond to a cubic perovskite structure. The patterns are in good agreement with the standard card PCPDF # 36001 and PCPDF # 00-001-1018.

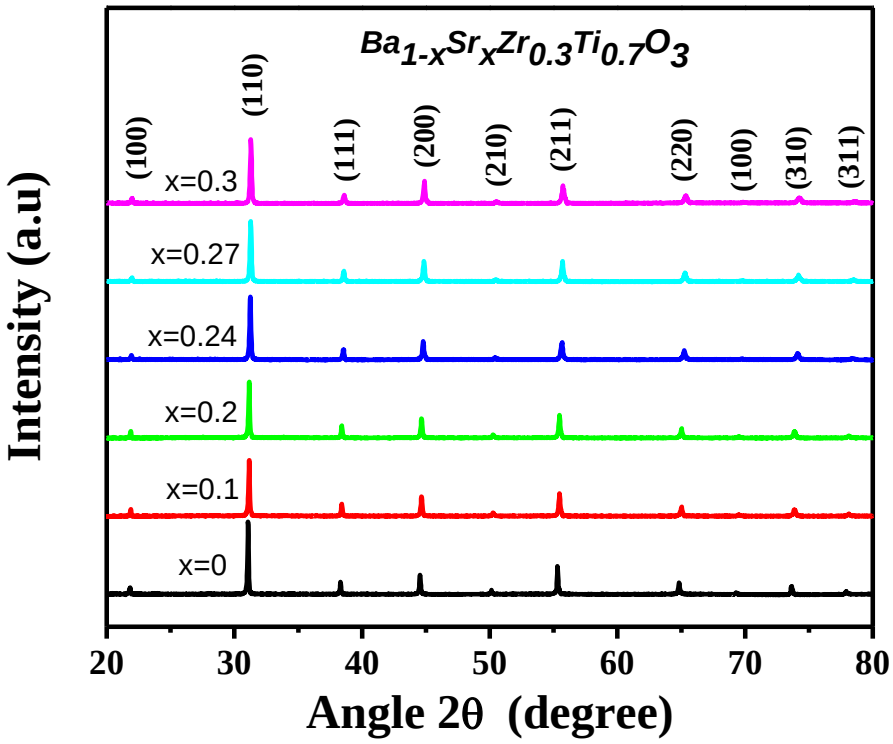

Figure 3.5: XRD Pattern of composition $Ba_{1-x}\,Sr_x\,Zr_{0.3}\,Ti_{0.7}O_3$

It is observed form the XRD-pattern that the principal diffraction peak shift toward the higher angle with increasing of Sr content. This shift is due to the incorporation of Smaller ionic radii Sr^{2+} (1.18 Å) in place of larger ionic radii Ba^{2+} (1.37 Å). The strains developed due to the difference on size of Sr^{2+} and Ba^{+2} cations. This is clear indication that the Sr is systematically dissolved in the $Ba\,Zr_{0.3}\,Ti_{0.7}\,O_3$ lattice in the studied compositions. No splitting of (200) peak is observed which reveal that the structure is cubic perovskite.

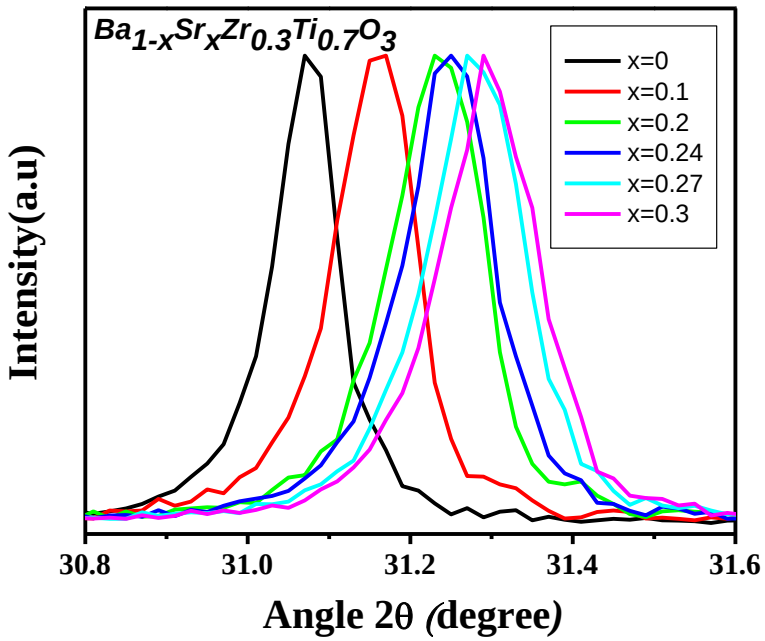

Figure 3.6: XRD peak variation of composition $Ba_{1-x}Sr_xZr_{0.3}Ti_{0.7}O_3$

The lattice constant of the sample was determined by the Eq. 3.4 and are listed in table 3.3. This data show a decrease in the lattice constant with increase in Sr content in the samples, the lattice is contract due to the smaller size of Sr ion. Figure 3.7 shows the graphical representation of the data in table 3.3.

Table 3.3: Values of the lattice parameter of $Ba_{1-x}Sr_xZr_{0.3}Ti_{0.7}O_3$ calculated from the XRD diffractogram.

x	$Ba_{1-x}Sr_xZr_{0.3}Ti_{0.7}O_3$	Lattice Parameter (Å)
0	$BaZr_{0.3}Ti_{0.7}O_3$	4.063 ± 0.001
0.1	$Ba_{0.9}Sr_{0.1}Zr_{0.3}Ti_{0.7}O_3$	4.053 ± 0.001
0.2	$Ba_{0.8}Sr_{0.2}Zr_{0.3}Ti_{0.7}O_3$	4.043 ± 0.001
0.24	$Ba_{0.76}Sr_{0.24}Zr_{0.3}Ti_{0.7}O_3$	4.042 ± 0.003
0.27	$Ba_{0.73}Sr_{0.27}Zr_{0.3}Ti_{0.7}O_3$	4.037 ± 0.002
0.3	$Ba_{0.7}Sr_{0.3}Zr_{0.3}Ti_{0.7}O_3$	4.035 ± 0.003

The variation in ρ_{XRD} as function of *Sr* concentration is shown in figure 3.7. From figure 3.7 it is observed that the ρ_{XRD} decreases with the addition of Sr^{+2} ion content, which is also attributed to the ionic radii of constituent ions causing decrease in lattice parameter.

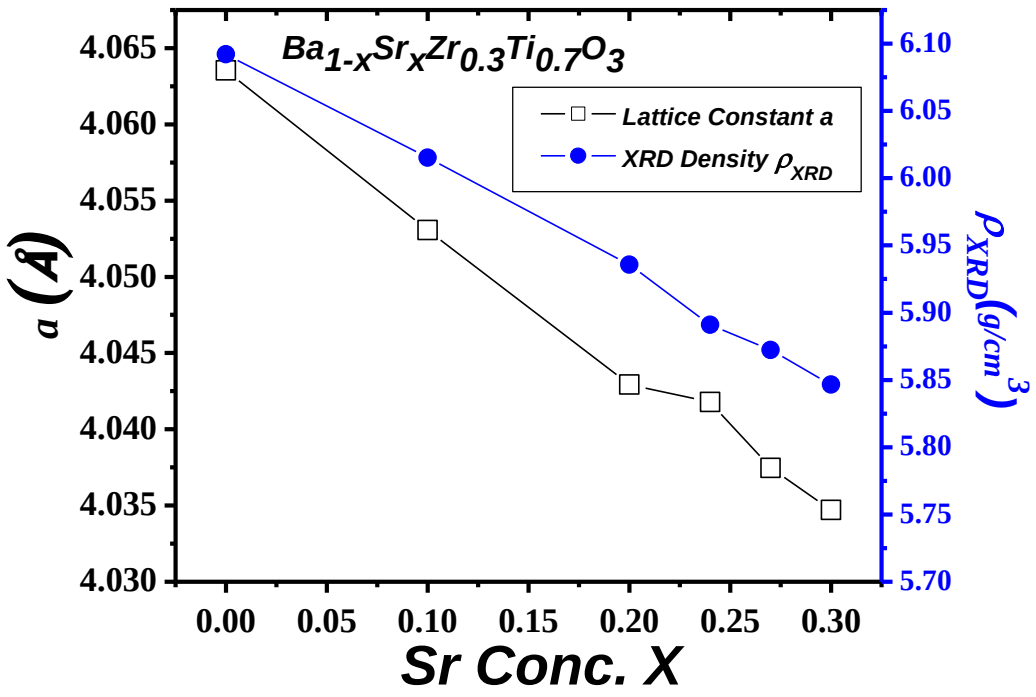

Figure 3.7: Lattice constant and ρ_{XRD} variation of composition $Ba_{1-x}Sr_xZr_{0.3}Ti_{0.7}O_3$

Chapter 4 RESULTS AND DISCUSSIONS

In this chapter we will present the dielectric properties of the ceramic compositions with general formula $Ba_{1-x}Sr_xZr_{0.2}Ti_{0.8}O_3$ (with $x = 0, 0.1, 0.2$ and 0.3) and $Ba_{1-x}Sr_xZr_{0.3}Ti_{0.7}O_3$ (with $x = 0, 0.1, 0.2, 0.24, 0.27, 0.3$). The motive is to search for new materials that have better ferroelectric properties. It is interesting to investigate these particular systems, whether the system exhibit a relaxor behavior with the increasing amount of Sr or not and what are the influence of Sr content addition in relaxor nature of this range of composition respectively. The details have been specified in Chapter 1.

The synthesis portion has already been described in chapter 3. Experimental part for $Ba_{1-x}Sr_xZr_{0.2}Ti_{0.8}O_3$ (with $x = 0, 0.1, 0.2$ and 0.3) consists of

- Temperature dependence of dielectric behaviour with the variation of *Sr (x)* at 500 kHz.
- Variation of dielectric constant with Sr concentration.
- Temperature dependence of dielectric behavior at different frequencies for all prepared compositions.
- Characterization of dielectric peak using Curie-Weiss behavior

Experimental part for $Ba_{1-x}Sr_xZr_{0.3}Ti_{0.7}O_3$ (with $x = 0, 0.1, 0.2, 0.24, 0.27$ and 0.3) consists of

- Temperature dependence of dielectric behavior with the variation of *Sr (x)* at 500 kHz
- Variation of dielectric constant with Sr concentration.
- Temperature dependence of dielectric behavior at different frequencies for all prepared compositions.
- Characterization of dielectric peak using Curie-Weiss behavior and Modified Curie – Weiss Law ($T > T'_m$).
- Temperature dependence of dielectric behavior at different frequencies for all prepared compositions.
- Freezing Temperature T_{VF} Calculation by means of Vögel- Fulcher Law.
- Superparaelectric Model: Edward–Anderson order parameter *q* with Sherrington and Kirkpatrick model.

4.1 Electrical Properties

The electrical measurements were carried out for ceramic compositions $Ba_{1-x}Sr_xZr_{0.2}Ti_{0.8}O_3$ (with *x =0, 0.1, 0.2 and 0.3*) and $Ba_{1-x}Sr_xZr_{0.3}Ti_{0.7}O_3$ (with *x =0, 0.1, 0.2, 0.24, 0.27 and 0.3*) at and below room temperature with different frequencies (0.2 kHz ≤ f ≤ 500 kHz). The dielectric measurements were performed with the help of four probes using Wayne Kerr LCR Meter Bridge (WK-4275) (see Chapter 2 for specifications). Both the capacitance "C" and dissipation factor "D" were studied.

The calibration of setup was done before taking the measurement on the sample. The principle of parallel plate capacitor was used for the measurement of dielectric constant. The dielectric constant (permittivity) of samples was calculated by using the relation.

$$\varepsilon' = \frac{Cd}{\varepsilon_o A} \qquad \textbf{4.1}$$

Where C is the capacitance of our sample, d is the distance (space) between plates and the sample was placed between the plates of capacitor, having area A. Here ε_o is the permittivity of free space. The dielectric constant ε is a complex quantity and shows the interaction of matter with an external electric field. The real part of dielectric constant (ε') shows the polarization features of the system under consideration. The imaginary part of dielectric constant (ε'') is a measure of how dissipative the matter is in relation to the electric field [44]. The imaginary part ε″ was calculated using relation.

$$\varepsilon'' = \varepsilon' \mathbf{D} \qquad \textbf{4.2}$$

Where D = tanδ, the dielectric loss.

4.1.1 Temperature dependence of dielectric constant of $Ba_{0.7}Sr_{0.3}Zr_{0.2}Ti_{0.8}O_3$

The temperature dependence of real and imaginary parts of dielectric constant of a sample $Ba_{0.7}Sr_{0.3}Zr_{0.2}Ti_{0.8}O_3$ is shown in figure 4.1. Where the measurement was taken at 500 kHz and, at 50*m*V applied AC field. The figure clearly shows that, increasing the temperature the real part and the imaginary part of dielectric permittivity increases gradually, reaches a broad maxima and then smoothly decrease. This dielectric behaviour is, understood to be due to a simultaneous structure transition (from orthorhombic to cubic) accompanied by a ferroelectric to a paraelectric transition.

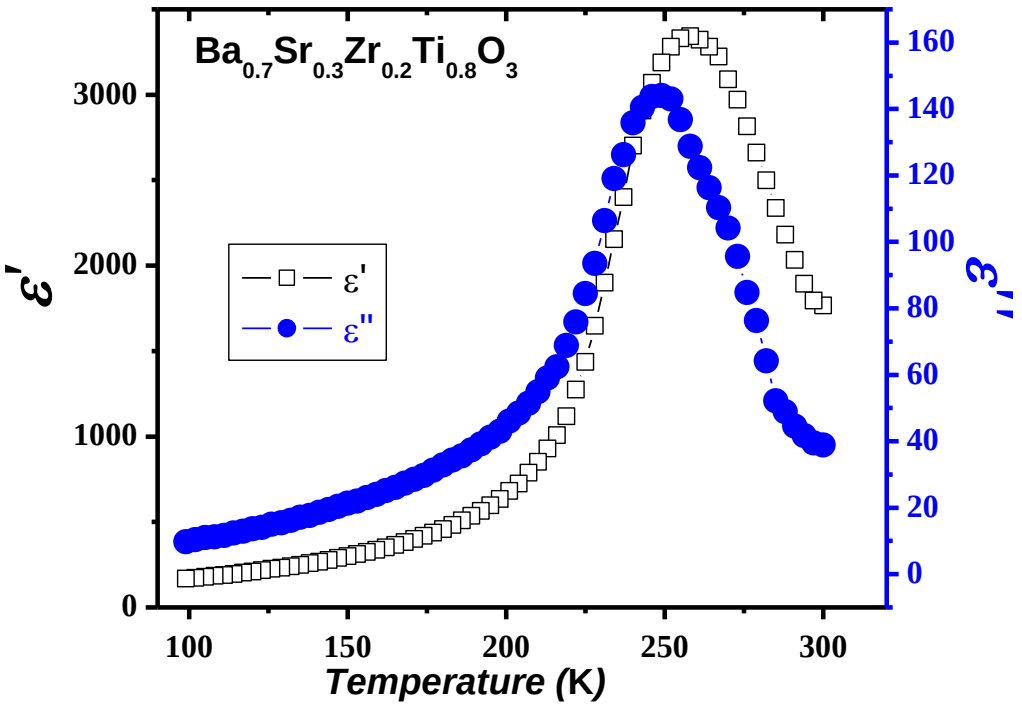

Figure 4.1: Temperature dependance of real and imaginary parts of dielectric permitivity

Similar measurements were also done for other composition and for different measuring frequencies these will be discussed later in section 4.1.4.

4.1.2 Dielectric permittivity, dielectric permittivity peaks and corresponding Temperature variation of $Ba_{1-x}Sr_xZr_{0.2}Ti_{0.8}O_3$

The real and imaginary parts of dielectric permitivty were measured for different Sr(x) concentration (with x=0, 0.1, 0.2, 0.3) at 500 kHz and, at 50*m*V Applied AC field. These results are shown in figure 4.2 and 4.3 respectivly. The data shown in these figures clearly ilustrate the effect of Sr substitution on the dielectric constant of BZT compound as a function of temperature. More precisely, the real and imaginary part of dielectric permtivty shows that the dielectric peak for these compounds increases with increasing Sr content (Fig.4.2 and 4.3). for example, the dielectric constant at T_m, reached a maximum of ~ 3459 at x=0.3 of Sr [45]. The detailed trend due to increasing Sr concentration in these componds is plotted in Fig.4.4, which shows a linear increase in the dielectric maxima with Sr concentration.

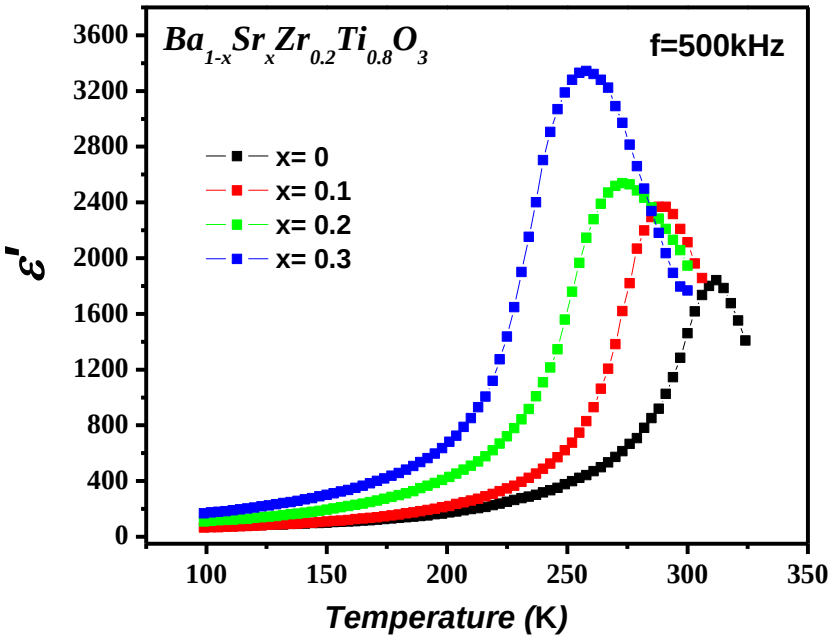

Figure 4.2: The real part of dielectric permitivity permitivity of various compositions (x = 0 to 0.3)

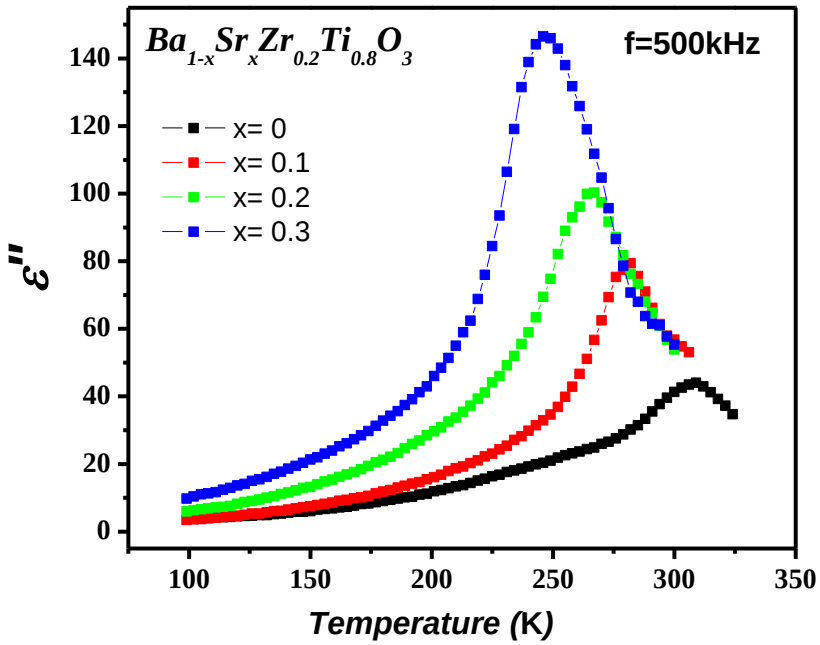

Figure 4.3: Imaginary part of dielectric permitivity of various compositions (x = 0 to 0.3)

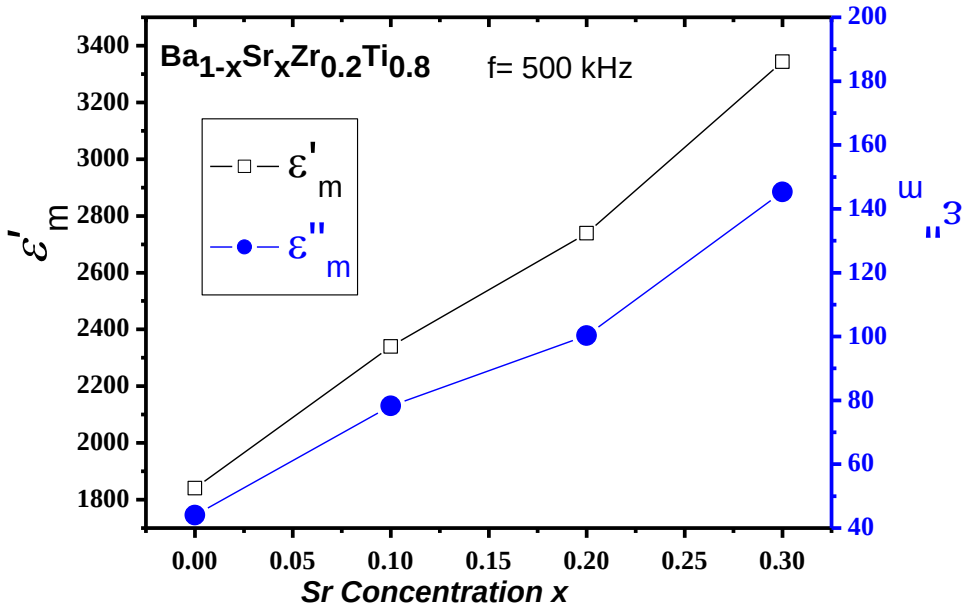

Figure 4.4: **Maxima of real and imaginary component of dielectric permitivty VS. Sr(x) concentration**

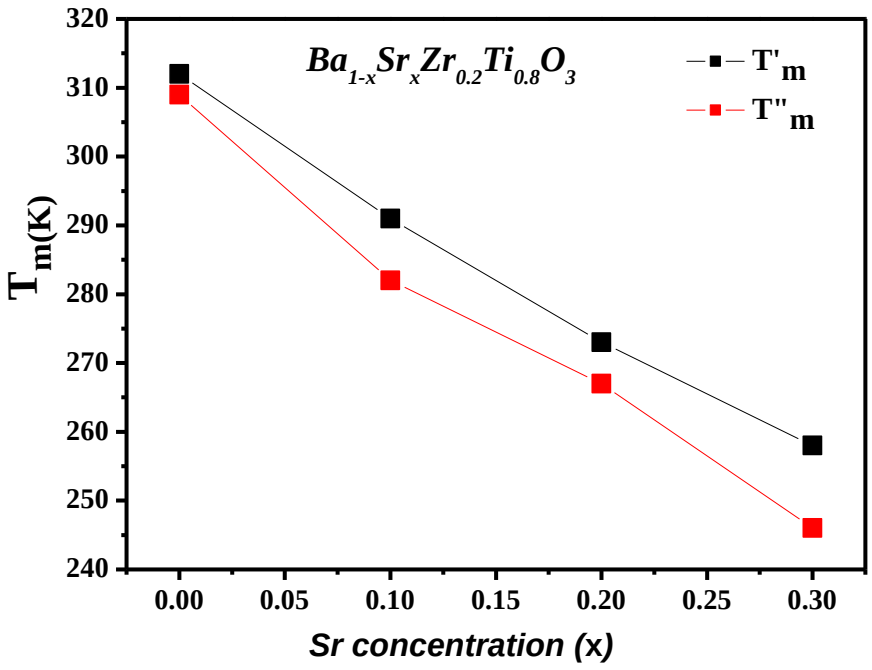

Figure 4.5: Corresponding Temprature for maxima of real and imaginary component of dielectric permitivty vs Sr(x) concentration

4.1.3 Reduced dielectric spectra of $Ba_{1-x}Sr_xZr_{0.2}Ti_{0.8}O_3$

The reduced dielectric spectra for both real and imaginary components of dielectric permitivity has been shown in figure 4.6 and figure 4.7 respectivley. The figure clearly shows that in every prepared composition there is an increase in a dielectric permitivity with increase in temprature. It could also be observed from figures that there is a gradual increase in the broadness of the peaks with increasing concentration of Sr(x) in BSZT. It has been argued that the broad transition may occur due to inhomogeneous distribution of Sr ions at the Ba site. In addition, mechanical stresses in the grain due to smaller Sr^{+2} ion may also lead to the broadening of the transition. The inhomogeneity in the compound arises due to the presence of number of voids and impurities of different sizes [1, 42, 46].

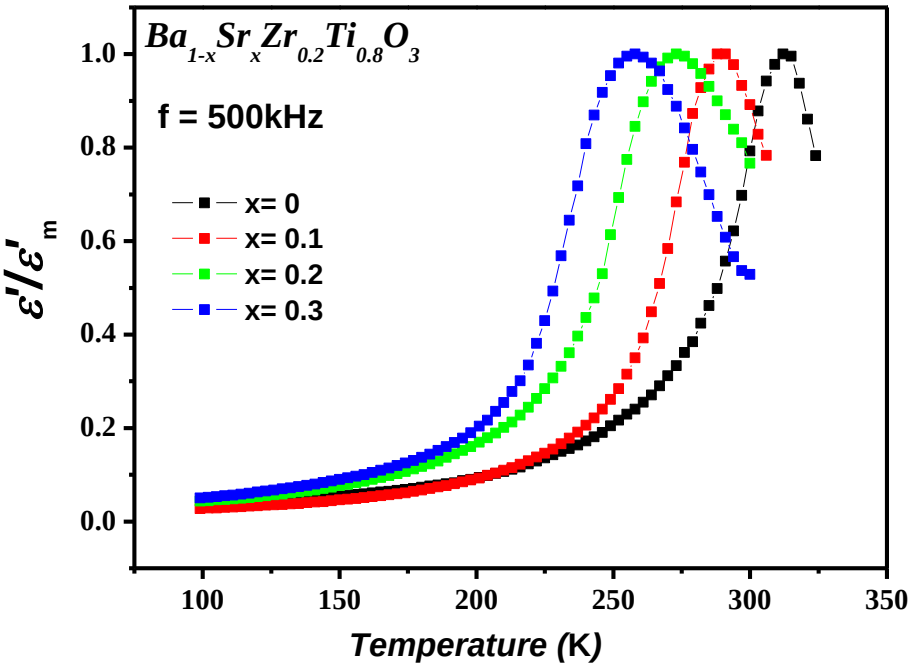

Figure 4.6: **Reduced dielectric spectra for real part of dielectric permitivity of $Ba_{1-x}Sr_xZr_{0.2}Ti_{0.8}O_3$ ($0 \leq x \leq 0.3$).**

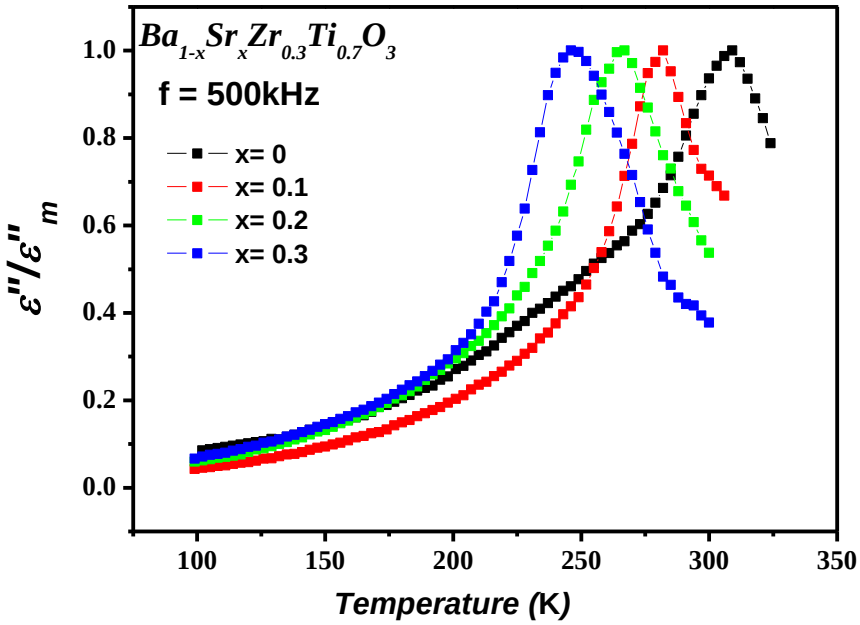

Figure 4.7: Reduced dielectric spectra for imaginary part of dielectric permitivity of $Ba_{1-x}Sr_xZr_{0.2}Ti_{0.8}O_3$ ($0 \leq x \leq 0.3$)

Moreover the analysis of figures indicates that there is an almost linear decrease in T_m , the temperature where the dielecric response shows maxima, for both real and imaginary parts of dielectric permitivity with increasing concentration of Sr(x) in BSZT system. The decrease might be due to the difference in the ionic raduis of Sr^{2+} and Ba^{2+} ions which has been shown to have smaller grain size and thus lower transition temperature [1, 42].

4.1.4 Temperature dependence of all prepared compositions of $Ba_{1-x}Sr_xZr_{0.2}Ti_{0.8}O_3$at different frequencies

The temperature dependence of the dielectric constant at different frequencies (1 to 500 kHz) have also been measured for all compositions of $Ba_{1-x}Sr_xZr_{0.2}Ti_{0.8}O_3$ (with x = 0, 0.1, 0.2 and 0.3) and are shown in fig 4.7 through fig 4.10. The real permittivity ε′ value gradually increases up to a maximum value ε'_m for all the $Ba_{1-x}Sr_xZr_{0.2}Ti_{0.8}O_3$ prepared compositions with the increase of temperature and then it smoothly decreases indicating the phase transition from ferroelectric to paraelectric state. A broad dielectric peaks has been observed in the vicinity of T'_m. The frequency dependent dielectric behavior illustrates

no dielectric dispersion for all prepared samples. All the samples have dielectric peaks (imaginary and real component) at same T_m that is there is no shifting of the peaks observed in any prepared compositions with different frequency [42]. The maximum values of real and imaginary components of dielectric permittivity are given in Table 4.1. Which clearly illustrate that with increasing frequency the maxima of real component of dielectric constant decreases, conversely the maxima of imaginary part of dielectric permittivity increasing with increasing frequency [47].

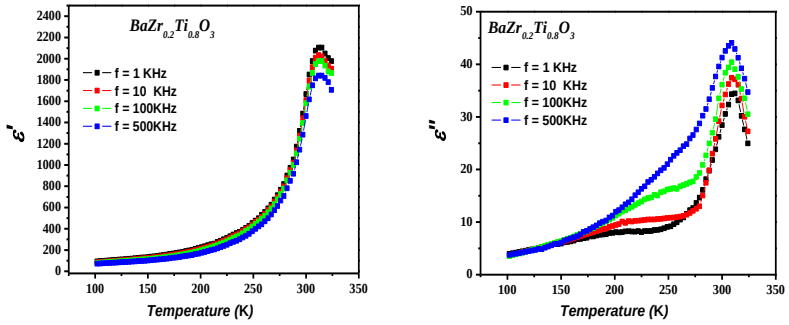

Figure 4.8: **Variation of ε' and ε'' of Ba$Zr_{0.2}Ti_{0.8}O_3$ with temperature at various frequencies**

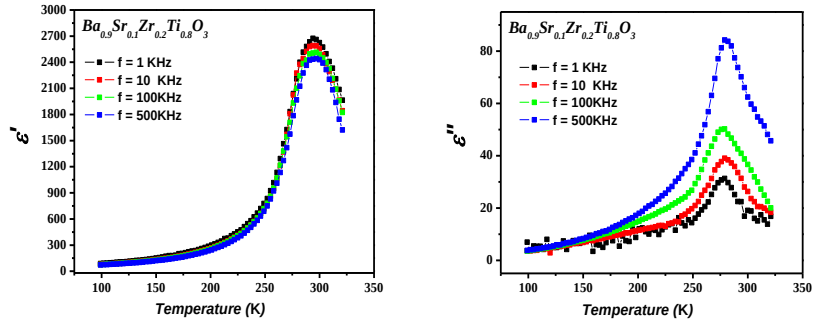

Figure 4.9: **Variation of ε' and ε'' of $Ba_{0.9}Sr_{0.1}Zr_{0.2}Ti_{0.8}O_3$ with temperature at various frequencies**

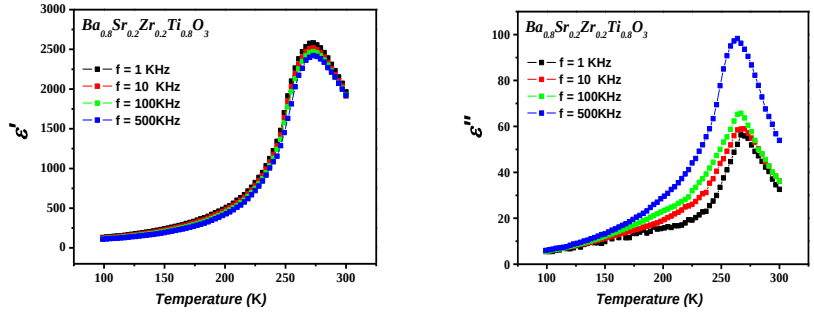

Figure 4.10: **Variation of ε' and ε'' of $Ba_{0.8}Sr_{0.2}Zr_{0.2}Ti_{0.8}O_3$ with temperature at various frequencies**

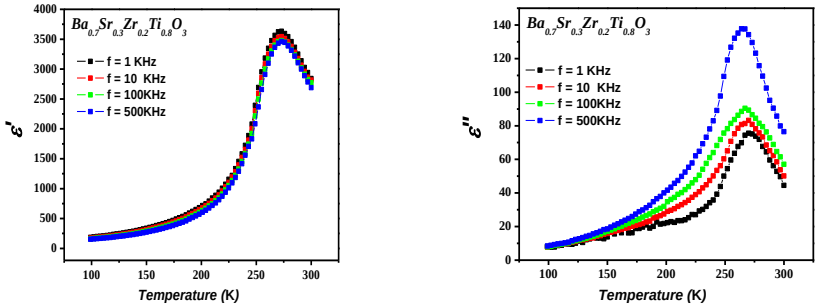

Figure 4.11: **Variation of ε' and ε'' of $Ba_{0.7}Sr_{0.3}Zr_{0.2}Ti_{0.8}O_3$ with temperature at various frequencies**

Table 4.1: **ε'_m and ε''_m values of $Ba_{1-x}Sr_xZr_{0.2}Ti_{0.8}O_3$ at various frequencies**

Composition	ε'_m				ε''_m			
	1 kHz	***10 kHz***	***100 kHz***	***500 kHz***	***1 kHz***	***10 kHz***	***100 kHz***	***500 kHz***
$BaZr_{0.2}Ti_{0.8}O_3$	2106	2038	1993	1849	34	37	40	44
$Ba_{0.9}Sr_{0.1}Zr_{0.2}Ti_{0.8}O_3$	2692	2600	2517	2435	31	39	51	84
$Ba_{0.8}Sr_{0.2}Zr_{0.2}Ti_{0.8}O_3$	2586	2524	2454	2409	57	59	66	98
$Ba_{0.7}Sr_{0.3}Zr_{0.2}Ti_{0.8}O_3$	3635	3545	3478	3459	76	82	91	138

Interestingly we observe that at low temperatures a second peak in ε'' is also visible. This second peak is more clearly observed at low data taken at low frequencies. Furthermore, it is also evident from the figures that this second peak becomes more prominent at low Sr concentrations. This has been observed by Reddy, S. B., K. P. Rao, et al. (2007) [45], they have attributed this to a further structural transitions. Based on detailed X-ray analysis, these authors argued that the structural transition from tetragonal to cubic in the parent sample (BZT) on Sr substitution goes throgh an intermediate transition such as the TOT (orthorhombic to tetragonal) and TRO (Rhombohedral to orthorhombic). However these transition are not observable in the real part of the dielectric permitivity. This is understandable due to sensitive nature of ε'' to dielectric response [45].

The decrease in the dielectric constant (ε'_m) can be clarified due to the origin of decrease in polarization with the increase in frequency. It's well recognized that, polarization of a dielectric material is the sum of the contributions of dipolar, electronic, ionic and interfacial polarizations. At low frequencies, all the polarizations react simply to

the time varying electric field but as the frequency of the electric field increases different polarization contributions screens out, as a consequence, the total polarization of the material decreases which shows the decrease in the value of ε'_m [42, 46].

4.2 Dielectric characterization of $Ba_{1-x}Sr_xZr_{0.3}Ti_{0.7}O_3$

AS discussed in chapter 1 and our prvious studies [Usman APL], the parent system namely, $BaZr_{0.3}Ti_{0.7}O_3$ shows a relaxor behavior that a diffused and frequecy dependent phase transtion. It is interesting to see how the relaor behaviour modifies if one replace the Ba ion with a smaller Sr ion. We have shown in chapter 3, that substitution of Sr with Ba produces smaller lattice constant and therefore it is expeced to have infuence in the competing polarization. The dielectric permitivity of compositions $Ba_{1-x}Sr_xZr_{0.3}Ti_{0.7}O_3$ (with x= 0, 0.1, 0.2, 0.24, 0.27, 0.3) has been conducted at various frequencies (f = 0.2-500 kHz). The overall charactrization of the BSZT0.3 system is given as follow:

4.2.1 Temperature dependence of dielectric constant of $Ba_{0.7}Sr_{0.3}Zr_{0.3}Ti_{0.7}O_3$

In figure 4.6, dielectric permitivity (both real and imaginary) have been ploted against temprature for BS0.3ZT0.3 sample at 500kHz and, at 50mV AC applied field. The figure clearly indicates that with increasing temprature the dielectric permitivty increases slowly and goes through a broad maxima, then with further increase in temprature the dielectric permitivty decreases smoothly indicating the phase transition. The broad maximum in the ε' is an important characteristic of the disordered perovskite structure with a diffuse phase transition (DPT). The imaginary part of dielectric constant that is proportional to the loss factor also shows a peak at the temperature where the slope *(ε' versus Temperature) is* or the variations in ε' are maximum. The maximum value of dielectric constant as determine from the graph is ε'_m (= 1856) and the temperature correspond to the peak values is T'_m (= 202.9 K). The maximum value of imaginary part is ε''_m (= 147) and the corresponding temperature is T''_m (= 175 K). Similar measurements were also performed for other composition and for different measuring frequencies these will be discussed later in section 4.2.3 [47].

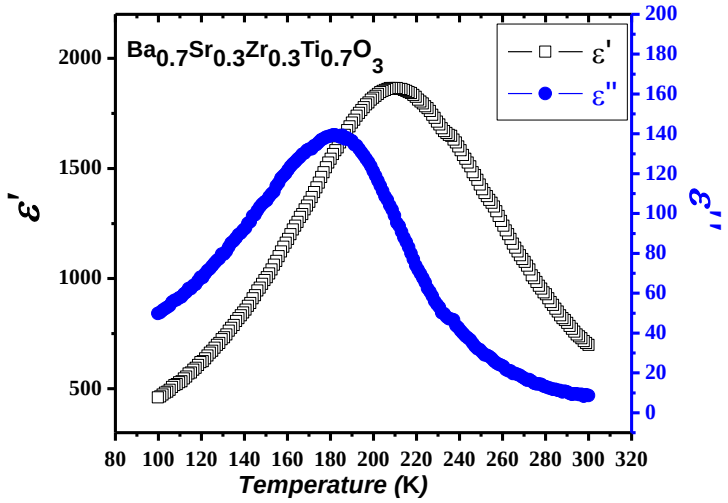

Figure 4.12: **Variation of ε' and ε'' of $Ba_{0.3}Sr_{0.1}Zr_{0.2}Ti_{0.8}O_3$ with temperature at 500 kHz**

4.2.2 Reduced dielectric spectra of dielectric permitivty ($\varepsilon'/\varepsilon'_m$ and $\varepsilon''/\varepsilon''_m$) at 500 kHz of $Ba_{1-x}Sr_xZr_{0.3}Ti_{0.7}O_3$

Figures 4.12 and 4.13 shows a reduced dielectric spectra of BSZT0.3 compositions vs temperature, measured at 500 kHz and, at 50mV apply AC field. It clearly shows the temperature dependency of the dielectric constant for various compositions. The value of dielectric permittivity increases gradually to a maximum value (ε'_m and ε''_m) with increase in temperature and passed a broad phase transition (diffused phase Transition) and then decreases smoothly. The observed diffused phase transition occurs mostly due to the compositional fluctuation and structural disordering in the positioning of cation in one or more crystallographic position of the structure. This indicates a microscopic inhomogeneity in the compound with different local curie points. As discussed earlier, the nature of this variation of dielectric permittivity suggest that the materials have paraelectric to ferroelectric phase transition [42, 46].

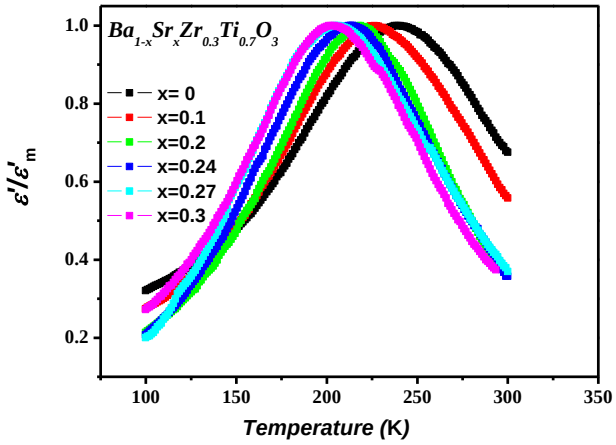

Figure 4.13: **Reduced dielectric spectra of real components of dielectric constant for all compositions at 500 kHz**

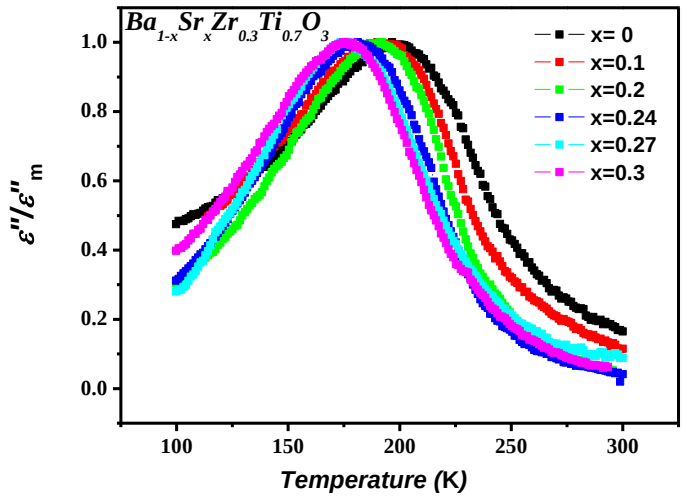

Figure 4.14: Reduced dielectric spectra of imaginary components of dielectric constant for all compositions at 500 kHz

Figure 4.14 shows Sr concentration dependence of the peak temperatures T'_m and T''_m of real and imaginary components of a dielectric constant ε'_m and ε''_m. There is a clear shift observed in a peak temperatures T'_m and T''_m towards low temperature as the Sr subsitution increases. The decrease in T'_m and T''_m might be due to a smaller ionic radius of Sr^{2+} than that of Ba^{2+} [46] as discussed in the previous sections.

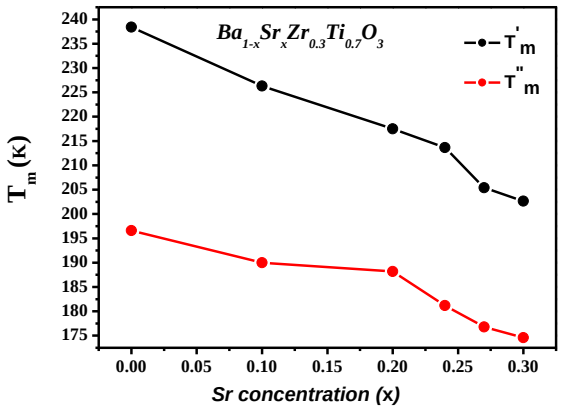

Figure 4.15: Coressponding dieletric peaks temptratures T_m vs. Sr concentraion at 500 kHz

From the figure 4.15 we note that the dielectric peaks increases as we increase the Sr content up to 24 % mol, however with further increase in the Sr contents results in the decrease in the dielectric maxima. At the moment we do not have a concrete explanation for the observed trend in dielectric constant with Sr concentration. However we note that the ferroelectrics with a large ionic displacement would have a high Curie temperature, a high spontaneous polarization and a high coercive field. The ionic displacements are effected by several factors containing (a) charge neutrality, (b) tolerance factor (t) where t is defined as $t = (r_A + r_o)/2(r_B + r_o)$ where r_A and r_B are the average radius of A and B site ions, respectively, and r_o is the ionic radius of oxygen, (c) ionic radius and (d) solubility/miscibility. The lattice distortion and compositional fluctuation caused in the parent doped BZT ceramic due to the introduction of Sr^{2+} ions in A-site could be a big reason for this kind of dielectric behavior [47]. We also note that the lattice constant as evaluated from xray diffraction studies (see fig. 3.7), shows a change of behavior or a discontinuity at the same position where the e' shows a decreasing trend with increasing Sr concentration. This may lead us to conclude that a solubility limit for Sr doping has reached and thereby breaking the long-range correlation in polarization and thus decreasing the dielectric maxima at after this Sr concentration. Same results were also observed at 0.2 kHz, 1 kHz, 10 kHz and 100 kHz (see section 4.1.3).

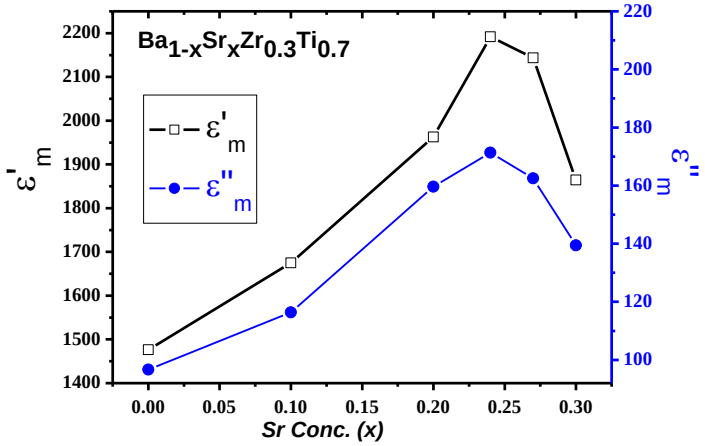

Figure 4.16: **Maxima of dielectric permitivities vs. Strontium (Sr) concentration**

4.2.3 Charactarization of Dielectric data using curie-wiess law and modified curie-weiss law

It has been found in the literature that the Curie Weiss Law is well represented by the high temperature dielectric permittivity for the ferroelectric (normal) materials as given in equation.

$$\frac{1}{\varepsilon'} = \frac{(T - Tcw)}{C} \qquad 4.3$$

Where *Tcw* is the Curie temperature and *C* is the Curie-Weiss constant but in case of relaxor ferroelectric the dielectric permittivity in paraelectric phase does not follow the Curie-Weiss law and a strong deviation is observed above the peak temperature [48].

Figure 4.16 shows plot of inverse dielectric permittivity versus temperature at frequency of 500 kHz for all prepared compositions $Ba_{1-x}Sr_xZr_{0.3}Ti_{0.7}O_3$ (with x= 0, 0.1, 0.2, 0.24, 0.27, 0.3). A deviation from Curie Weiss law can be seen in all stated compositions. The parameter Tm, which expresses the degree of the deviation from the Curie Weiss law is defined as, $\Delta T_m = T_{dev} - T_m$ where T_{dev} denotes the temperature from which the dielectric constant starts to deviate from the Curie Weiss law where T_m represents the temperature of the dielectric maximum. The fitted data is shown in fig. 4.16.

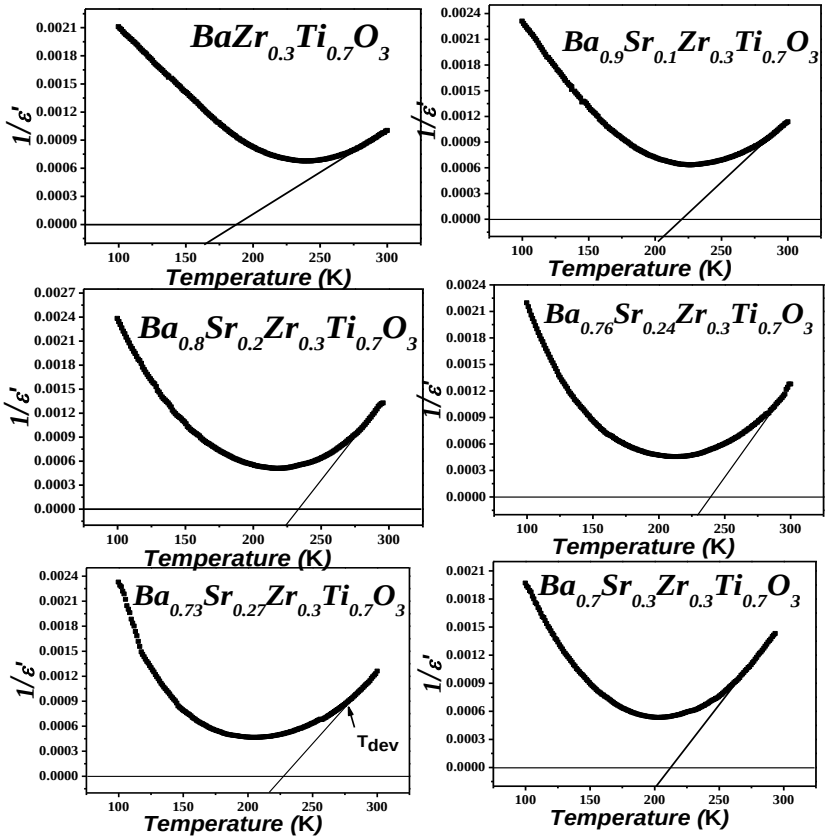

Figure 4.17: **Curie wiess law fitting to all prepared composition at 500 kHz**

The Curie temperature is found from the graph by extrapolation of the reciprocal of dielectric constant of a paraelectric state. The parameters found after fitting the experimental data are given in Table 4.2.

Table 4.2: **Curie wiess law parameters**

Sample	**C**	T_{cw} **(K)**	T_{dev} **(K)**	T_m **(K)**	ΔT_m **(K)**
$BaZr_{0.3}Ti_{0.7}O_3$	1.11×10^5	228 ± 2	264	238	36
$Ba_{0.9}Sr_{0.1}Zr_{0.3}Ti_{0.7}O_3$	1.6×10^5	220 ± 1	253	226	33
$Ba_{0.8}Sr_{0.2}Zr_{0.3}Ti_{0.7}O_3$	1.91×10^5	213 ± 2	244	218	31
$Ba_{0.76}Sr_{0.24}Zr_{0.3}Ti_{0.7}O_3$	1.97×10^5	209 ± 2	239	214	30
$Ba_{0.73}Sr_{0.27}Zr_{0.3}Ti_{0.7}O_3$	1.98×10^5	206 ± 1	235	206	29
$Ba_{0.7}Sr_{0.3}Zr_{0.3}Ti_{0.7}O_3$	2.05×10^5	205 ± 2	231	202	26

It is evident from the table that T_{cw} decrease as the Sr subsitution increases in parent compound. This trend is similar to Tm, observed in all prepared samples.

Note that for the relaxor ferroelectrics that display DPT the overall fit of data from high temperature up to *T'm* is typically expressed by modified Curie–Weiss Law [22, 49, 50]. The modified Curie-Weiss law can be stated as

$$\frac{1}{\varepsilon'} = \frac{1}{\varepsilon'_m} + \frac{(T - T'_m)^{\gamma}}{C_1} \qquad \textbf{4.4}$$

By solving the last equation we get

$$\ln\left(\frac{1}{\varepsilon'} - \frac{1}{\varepsilon'_m}\right) = \gamma \ln\left(T - T_m\right) - \ln C_1$$

The above equation represnts the equation of straight line having slope = γ and with

$$y = \ln\left(\frac{1}{\varepsilon'} - \frac{1}{\varepsilon'_m}\right) \qquad \text{And} \qquad x = \ln\left(T - T_m\right)$$

From the intercept we get the value of C_1 and the slope of the equation give the value of γ. The graphical solution of the Equation 5.4 by log-log plot i.e. $\ln\left(1/\varepsilon' - 1/\varepsilon'_m\right)$ vs. $\ln\left(T - T'_m\right)$ as shown in Figure 4.17. Scatter points represent the experimental data and line on the graph indicates the modified Curie-Weiss law fit.

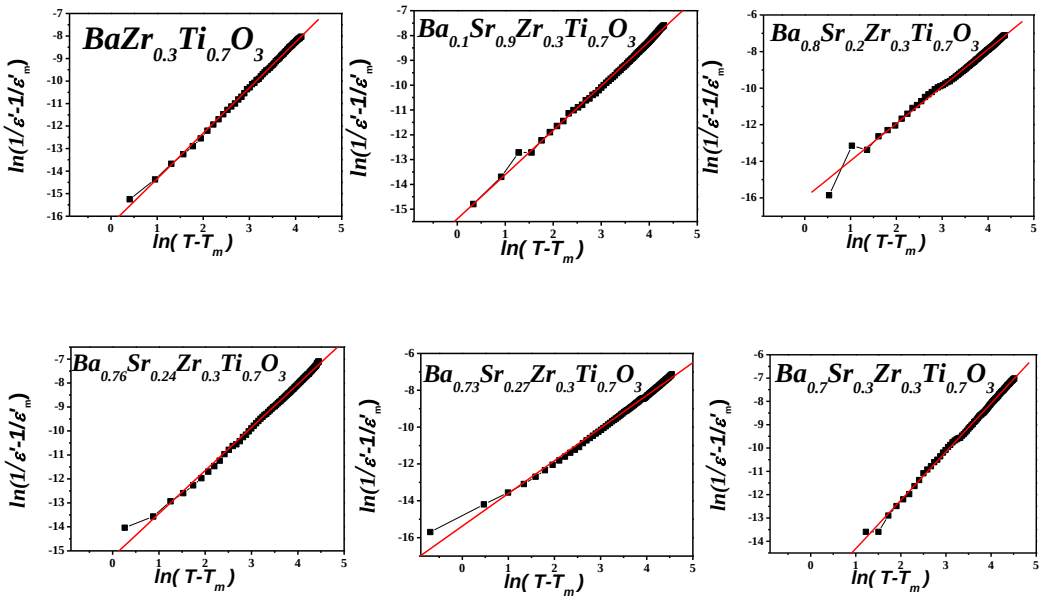

Figure 4.18 : **Modefied crie wiess law fitting to all prepared compositions at 500 kHz.**

Table 4.3: **Modefied curie wiess law parameters**

$Ba_{1-x}Sr_xZr_{0.3}Ti_{0.7}O_3$	C_1	γ
$BaZr_{0.3}Ti_{0.7}O_3$	1×10^6	1.98
$Ba_{0.9}Sr_{0.1}Zr_{0.3}Ti_{0.7}O_3$	8.2×10^6	1.92
$Ba_{0.8}Sr_{0.2}Zr_{0.3}Ti_{0.7}O_3$	8.8×10^6	1.97
$Ba_{0.76}Sr_{0.24}Zr_{0.3}Ti_{0.7}O_3$	7.3×10^6	1.89
$Ba_{0.73}Sr_{0.27}Zr_{0.3}Ti_{0.7}O_3$	7.5×10^6	1.91
$Ba_{0.7}Sr_{0.3}Zr_{0.3}Ti_{0.7}O_3$	9.03×10^6	1.98

The parameter γ gives information about the character of the phase transition; for $\gamma = 1$, a normal Curie Weiss law is obtained; for $\gamma = 2$, it reduces to the quadratic dependency which describes a complete diffuse phase transition. For a fixed temperature range an increase of the parameters for the compositions with increasing Sr content was reported [42, 46].

4.2.4 Temprature dependance of all prepared compositions of $Ba_{1-x}Sr_xZr_{0.3}Ti_{0.7}O_3$ at different frequencies.

The temperature dependence of both the real and imaginary part of dielectric permittivity of $Ba_{1-x}Sr_xZr_{0.3}Ti_{0.7}O_3$ composition with $0 \leq x \leq 0.3$ at several frequencies are shown in Fig. 4.18-23.

All the composition shows a similar behavior for both real and imaginary parts of dielectric constant with increasing temperature. It is clear that with increasing temperature the dielectric permittivity increases slowly and passed through a broad maxima indicating the Diffused type of phase transition (DPT) and with further increase in temperature it decreases smoothly.

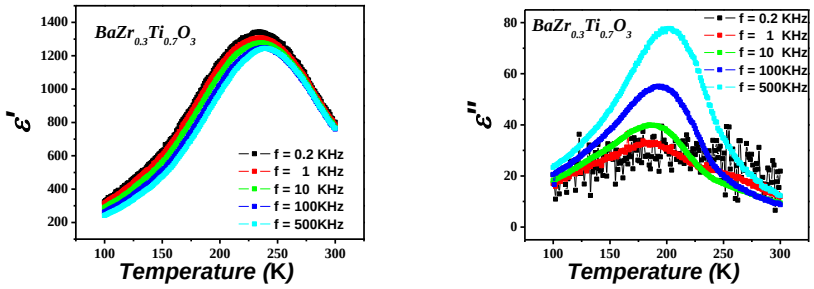

Figure 4.19: Variation of ε' and ε'' of $BaZr_{0.3}Ti_{0.7}O_3$ with temperature at various frequencies

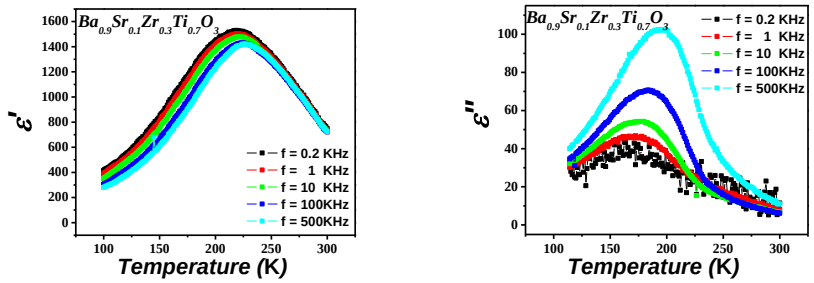

Figure 4.20: Variation of ε' and ε'' of $Ba_{0.9}Sr_{0.1}Zr_{0.3}Ti_{0.7}O_3$ with temperature at various frequencies

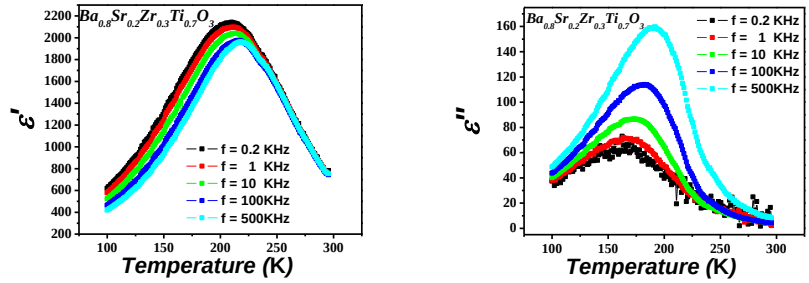

Figure 4.21: Variation of ε' and ε'' of $Ba_{0.8}Sr_{0.2}Zr_{0.3}Ti_{0.7}O_3$ with temperature at various frequencies

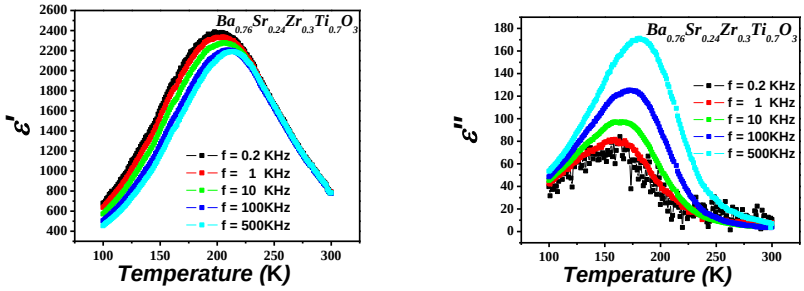

Figure 4.22: Variation of ε' **and** ε'' **of** $Ba_{0.76}Sr_{0.24}Zr_{0.3}Ti_{0.7}O_3$ **with temperature at various frequencies**

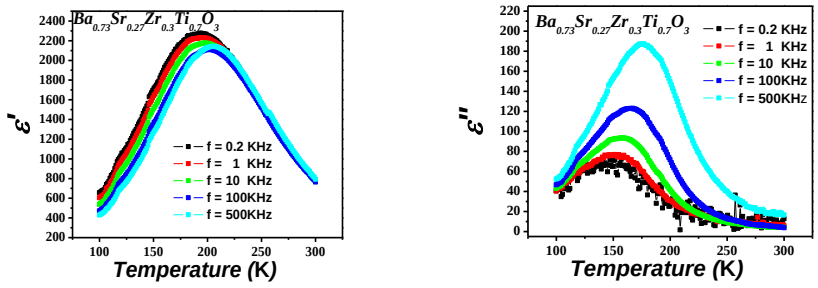

Figure 4.23: **Variation of ε' and ε'' of $Ba_{0.73}Sr_{0.27}Zr_{0.3}Ti_{0.7}O_3$ with temperature at various frequencies**

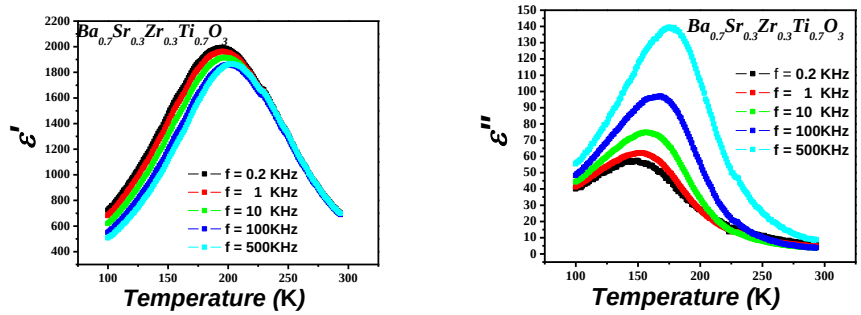

Figure 4.24: **Variation of ε' and ε'' of $Ba_{0.7}Sr_{0.3}Zr_{0.3}Ti_{0.7}O_3$ with temperature at various frequencies**

It is worth noteing from the figures that dielectric permitivity maxima (ε'_m and ε''_m) shows strong dispersion. This dispersion in the system is the key feautre for the relxor ferroelectric system. It is clear from the figures that as we increase the frequency, the real part of dielectric permittivity maxima (ε'_m) decreases and the corresponding peak temprature (T'_m) shifts toward high temprature.

However, in case of imaginary permitivity maxima (ε''_m), with increasing frequency it increases and corresponding peak temprature (T''_m) shifts toward higher temprature. Which is also consistent to the relaxation–type behavior in the dielectric polarization as detected in dipolar glasses. The measured value of ε'_m and ε''_m and corresponding T'_m and T''_m for all prepared compositions at various frequencies are given in Table 4.4, 4.5.

Table 4.4: **Maxima of dielectric permitivities at various frequencies of $Ba_{1-x}Sr_xZr_{0.3}Ti_{0.7}O_3$**

Composition	ε'_m					ε''_m				
	0.2 kHz	***1 kHz***	***10 kHz***	***100 kHz***	***500 kHz***	***0.2 kHz***	***1 kHz***	***10 kHz***	***100 kHz***	***500 kHz***
$BaZr_{0.3}Ti_{0.7}O_3$	134	1306	1276	1248	1243	30	33	40	55	78
$Ba_{0.9}Sr_{0.1}Zr_{0.3}Ti_{0.7}O$	153	1501	1478	1429	1421	39	46	55	71	102
$Ba_{0.8}Sr_{0.2}Zr_{0.3}Ti_{0.7}O$	214	2097	2040	1976	1962	63	71	86	114	159
$Ba_{0.76}Sr_{0.24}Zr_{0.3}Ti_{0.7}$	237	2336	2277	2204	2190	71	79	97	125	170
$Ba_{0.73}Sr_{0.27}Zr_{0.3}Ti_{0.7}$	227	2231	2176	2109	2100	67	76	93	123	187
$Ba_{0.7}Sr_{0.3}Zr_{0.3}Ti_{0.7}O$	199	1964	1916	1860	1856	57	62	74	97	147

Table 4.5: Corresponding temprature of Maximum of dielectric permitivities at various frequencies of $Ba_{1-x}Sr_xZr_{0.3}Ti_{0.7}O_3$

Composition	T'_m					T''_m				
	0.2 kHz	***1 kHz***	***10 kHz***	***100 kHz***	***500 kHz***	***0.2 kHz***	***1 kHz***	***10 kHz***	***100 kHz***	***500 kHz***
$BaZr_{0.3}Ti_{0.7}O_3$	230	232	234	236	238	183	185	188	194	202
$Ba_{0.9}Sr_{0.1}Zr_{0.3}Ti_{0.7}O_3$	218	219	221	224	226	169	174	178	184	195
$Ba_{0.8}Sr_{0.2}Zr_{0.3}Ti_{0.7}O_3$	209	210	213	214	217	165	169	176	183	191
$Ba_{0.76}Sr_{0.24}Zr_{0.3}Ti_{0.7}O$	203	204	205	209	212	160	163	166	172	182
$Ba_{0.73}Sr_{0.27}Zr_{0.3}Ti_{0.7}O$	193	194	197	200	205	152	155	157	166	176
$Ba_{0.7}Sr_{0.3}Zr_{0.3}Ti_{0.7}O_3$	191	192	195	197	200	143	151	157	168	147

The observed broadness or diffusiveness in the dielectric response follow mostly due to the compositional fluctuation and structural disordering in the positioning of cations in one or more crystallographic site of the structure. This proposes a microscopic inhomogeneity in the compound with various local curie points.

The properties of relaxors are closely linked to their unique polar structure, namely to the presence of polar clusters of nanometer-size, which has a net dipole moment (each). These polar clusters are called polar nano regions (PNRs). These PNRs are supposed as divided regions of nanometer size keeping a spontaneous polarization (P_S) and having a characteristic relaxation time controlled by the local field configuration. The dielectric response is understood as an effect of reorientation of the local polarization vectors in a result of applied electric filed [28].

4.2.5 Calculation of freezing temperature (T_{VF}) and activation energy (E_a) using Vogel-Fulcher law

It t is supposed that short range interaction among PNRs controls the fluctuations of polarization, P_S, this results to the freezing of polar nano regions (PNRs) at a characteristic temperature (T_{VF}) and so the transition into the glass likes state. To explain more precisely this we have plotted *ln(f)* vs. T'_m of $Ba_{1-x}Sr_xZr_{0.3}Ti_{0.7}O_3$ composition with $0 \leq x \leq 0.3$ as shown in figure 4.24. In order to investigate the relaxation features, the experimental curves were fitted using the Vogel-Fulcher law as follow

$$f = f_o \exp\left[-\frac{E_a}{k_B(T_m - T_{VF})}\right] \quad \textbf{4.5}$$

Where f_o is the attempt frequency, E_a is the amount of average activation energy, and k_B is the Boltzman constant, and T_{VF} is the freezing temperature. T_{VF} is considered as the temperature where the dynamic reorientation of the dipolar cluster polarization can no longer be thermally activated [42, 46]. The value of average activation energy and freezing temperature for all compositions are given in Table 4.6.

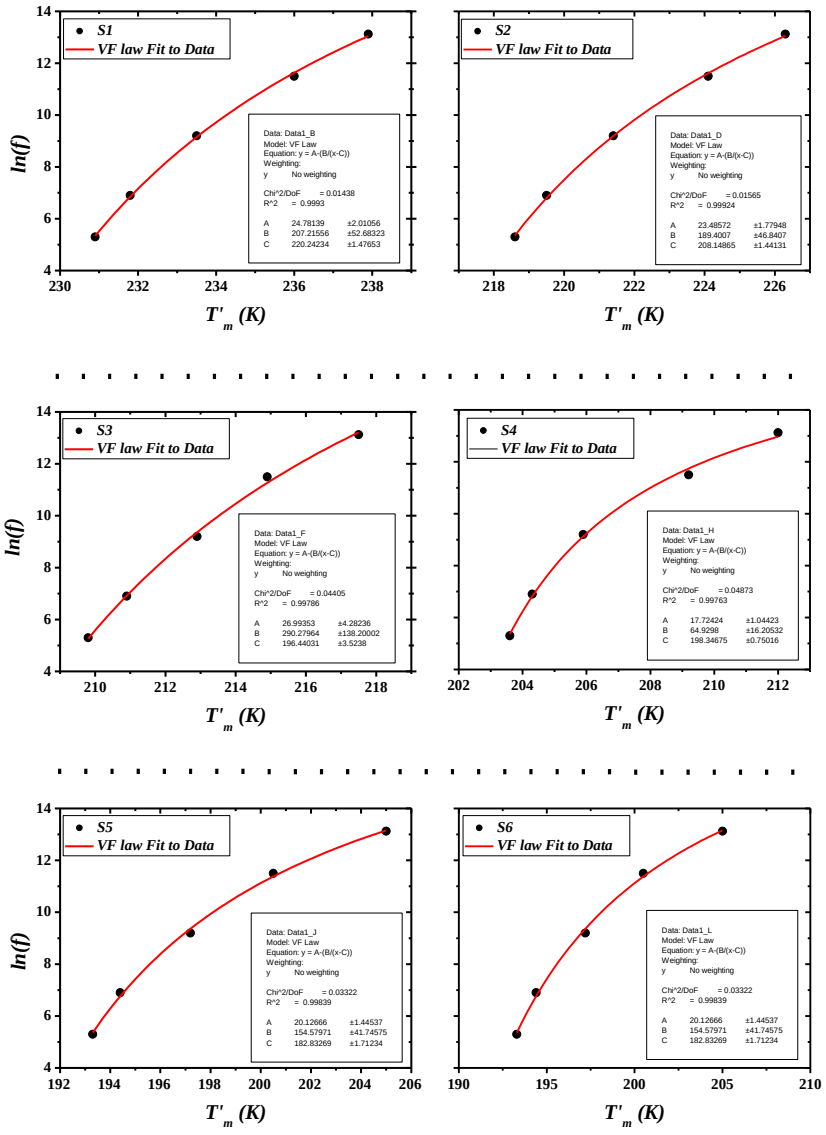

Figure 4.25: **Vogel-Fulcher law fitting to the experimental data of $Ba_{1-x}Sr_xZr_{0.3}Ti_{0.7}O_3$ composition with $0 \leq x \leq 0.3$**

From the values in table there is a close agreement of the data with the V–F relationship proposes the relaxor behavior in the system. The decrease in activation energy may be due to decrease in grain size caused from Sr replacement in place of Ba [42].

Table 4.6: **Freezing Temprature (T_{VF})and average activation energy (E_a) of $Ba_{1-x}Sr_xZr_{0.3}Ti_{0.7}O_3$ composition with $0 \leq x \leq 0.3$**

$Ba_{1-x}Sr_xZr_{0.3}Ti_{0.7}O_3$	T_{VF} (K)	E_a (meV)
$BaZr_{0.3}Ti_{0.7}O_3$	216	17.8
$Ba_{0.9}Sr_{0.1}Zr_{0.3}Ti_{0.7}O_3$	208	16.3
$Ba_{0.8}Sr_{0.2}Zr_{0.3}Ti_{0.7}O_3$	198	14.5
$Ba_{0.76}Sr_{0.24}Zr_{0.3}Ti_{0.7}O_3$	196	13
$Ba_{0.73}Sr_{0.27}Zr_{0.3}Ti_{0.7}O_3$	183	11.6
$Ba_{0.7}Sr_{0.3}Zr_{0.3}Ti_{0.7}O_3$	183	11.6

4.3 Summary and Conclusion

The ceramic compositions with general formula $Ba_{1-x}Sr_xZr_{0.2}Ti_{0.8}O_3$ (with $x = 0, 0.1, 0.2$ and 0.3) were synthesized following the solid state reaction route. The room temperature X-ray diffraction spectra of ($Ba_{1-x}Sr_xZr_{0.2}Ti_{0.8}O_3$) samples were found to be single phase and correspond to a perovskite structure. The temperature dependency dielectric study on the composition $Ba_{1-x}Sr_xZr_{0.2}Ti_{0.8}O_3$ (with $x = 0, 0.1, 0.2$ and 0.3) was carried out in the temperature range 300 K to 100 K. No frequency dispersion is detected around the ε'_m and ε''_m peak for all the $Ba_{1-x}Sr_xZr_{0.2}Ti_{0.8}O_3$ compositions. Similarly in all the $Ba_{1-x}Sr_xZr_{0.2}Ti_{0.7}O_3$ compositions that, with increasing frequency ε' decreases and there is no shift observed in T'_m where the ε'_m occur. Which clearly identify that there is no relaxor type behaviour in the system. In a similar manner the temperature of the loss maxima (ε''_m) increases with increase in frequency however peak value increases unlike ε'_m. The increase in magnitude of ε'_m and ε''_m is observed for all compositions of $Ba_{1-x}Sr_xZr_{0.2}Ti_{0.8}O_3$ with increase in Sr content. Similarly the shift in transition temperature towards low temperature is also observed with increasing concentration of Sr in a $Ba_{1-x}Sr_xZr_{0.2}Ti_{0.8}O_3$ system.

The ceramic compositions with general formula $Ba_{1-x}Sr_xZr_{0.3}Ti_{0.7}O_3$ (with $x = 0, 0.1, 0.2$, 0.24, 0.27 and 0.3) were synthesized following the solid state reaction route. The room temperature X-ray diffraction spectra of ($Ba_{1-x}Sr_xZr_{0.3}Ti_{0.7}O_3$) samples were found to be single phase and correspond to a perovskite structure. The temperature dependency dielectric study on the composition $Ba_{1-x}Sr_xZr_{0.2}Ti_{0.7}O_3$ (with $x = 0, 0.1, 0.2, 0.24, 0.27$ and 0.3) was carried out in the temperature range 300 K to 100 K. The strong frequency dispersion is detected around the vicinity of ε'_m and ε''_m peak for all the $Ba_{1-x}Sr_xZr_{0.3}Ti_{0.7}O_3$

compositions. Similarly in all the $Ba_{1-x}Sr_xZr_{0.3}Ti_{0.7}O_3$ compositions that, with increasing frequency ε' decreases and there is a strong shift observed in T'_m where the ε'_m occur. Which clearly signals that the relaxor type behaviour in the system and indicating a diffuse type of phase transition. In a similar manner the temperature of the loss maxima (ε''_m) increases with increase in frequency however peak value increases unlike ε'_m. which is also attributed to the relaxor type behaviour in the system. The increase in magnitude of ε'_m and ε''_m is observed for x=0 to x=0.24 of $Ba_{1-x}Sr_xZr_{0.2}Ti_{0.8}O_3$ and then for x=0.27 and x=0.3, the magnitude of ε'_m and ε''_m is observed to be decreased. Similarly the shift in transition temperatures towards low temperature is also observed with increasing concentration of Sr in a $Ba_{1-x}Sr_xZr_{0.2}Ti_{0.8}O_3$ system.

A strong deviation from Curie-Weiss law at T_{dev} is detected for all the compositions. To study the diffuseness, the data were fitted with a modified Curie-Weiss law and the degree of diffuseness were also calculated. We have found that how the relaxor behavior has gradually been developed with the increasing substitution of Sr^{+2} ions for the Ba^{+2} in the matrix of *BZT0.3*. Relaxor behavior becomes more advances with the increase in content of Sr^{+2} ions i.e. with growing amount of the Polar Regions. The dielectric relaxations in BSZT system are found to follow Vogel-Fulcher type behavior (initially derived for the spin-glass materials) and the experimental data were found to be in good agreement with the theoretical fitting.

.

References

1. Badapanda, T., et al., *Optical and dielectric study of strontium modified barium zirconium titanate ceramic prepared by high energy ball milling.* Journal of Alloys and Compounds, 2015. **645**: p. 586-596.
2. Huang, H.-H., et al., *Evaluation on Structure Modification and Properties of (Ba1-xSrx)(Ti1-y Zry) O3 Ceramics by using Rietveld Method*. 2011: INTECH Open Access Publisher.
3. Kittel, C., *Introduction to solid state physics*. 2005: Wiley.
4. Valasek, J., *Piezo-electric and allied phenomena in Rochelle salt.* Physical review, 1921. **17**(4): p. 475.
5. Valasek, J., *Piezo-Electric and Allied Phenomena in Rochelle Salt.* Physical Review, 1921. **17**: p. 475-481.
6. Matthias, B. and A. Von Hippel, *Domain structure and dielectric response of barium titanate single crystals.* Physical Review, 1948. **73**(11): p. 1378.
7. Cross, L.E., *Relaxor ferroelectrics.* Ferroelectrics, 1987. **76**(1): p. 241-267.
8. Von Hippel, A., *Ferroelectricity, domain structure, and phase transitions of barium titanate.* Reviews of Modern Physics, 1950. **22**(3): p. 221.
9. Lines, M.E. and A.M. Glass, *Principles and applications of ferroelectrics and related materials*. 1977: Oxford university press.
10. 上田隆三, *HD Megaw: Ferroelectricity in Crystals., Methuen & Co., 1957, 211 頁, 14× 22cm, 27s. 6d.* 日本物理學會誌, 1958. **13**(5): p. 340-341.
11. Nettleton, R., *Ferroelectric phase transitions: A review of theory and experiment. Part 3—neutron scattering.* Ferroelectrics, 1970. **1**(1): p. 93-101.
12. Tidrow, S.C., *Mapping comparison of Goldschmidt's tolerance factor with Perovskite structural conditions.* Ferroelectrics, 2014. **470**(1): p. 13-27.
13. Uchino, K., *Piezoelectrics and ultrasonic applications*. 1998, Kluwer, Deventer.
14. Tadigadapa, S. and K. Mateti, *Piezoelectric MEMS sensors: state-of-the-art and perspectives.* Measurement Science and technology, 2009. **20**(9): p. 092001.
15. Moon, J., et al., *Formation mechanisms and morphological changes during the hydrothermal synthesis of BaTiO 3 particles from a chemically modified, amorphous titanium (hydrous) oxide precursor.* Journal of the European Ceramic Society, 2003. **23**(12): p. 2153-2161.
16. Kinoshita, K. and A. Yamaji, *Grain-size effects on dielectric properties in barium titanate ceramics.* Journal of Applied Physics, 1976. **47**(1): p. 371-373.
17. Burns, G. and F. Dacol, *Ferroelectrics with a glassy polarization phase.* Ferroelectrics, 1990. **104**(1): p. 25-35.
18. Merz, W.J., *Domain Formation and Domain Wall Motions in Ferroelectric BaTi O 3 Single Crystals.* Physical Review, 1954. **95**(3): p. 690.
19. Safari, A., R. Panda, and V. Janas. *Ferroelectricity: Materials, characteristics & applications*. in *Key Engineering Materials*. 1996: Trans Tech Publ.
20. Jaffe, B., *W. Cook and H. Jaffe, Piezoelectric Ceramics*. 1971, Academic Press, London.
21. Xu, Y., *Ferroelectric materials and their applications*. 2013: Elsevier.
22. Stenger, C. and A. Burggraaf, *Study of phase transitions and properties of tetragonal (Pb, La)(Zr, Ti) O3 ceramics—II: Diffuse phase transitions and thermodynamics.* Journal of Physics and Chemistry of Solids, 1980. **41**(1): p. 25-30.
23. Känzig, W., *Röntgenuntersuchungen über die Seignetteelektrizität von Bariumtitanat*. 1951, Diss. Naturwiss. ETH Zürich, Nr. 1997, 1951, 0000. Ref.: Scherrer, P.; Korref.: Busch, G.
24. Lin, Y. and A. Burggraaf, *Modelling and analysis of CVD processes in porous media for ceramic composite preparation.* Chemical engineering science, 1991. **46**(12): p. 3067-3080.

25. Smolenskii, G.A.e., *Physical phenomena in ferroelectrics with diffused phase transition.* J. Phys. Soc. Jpn, 1970. **28**(1): p. 26-37.
26. Smolensky, G., *Ferroelectrics with diffuse phase transition.* Ferroelectrics, 1984. **53**(1): p. 129-135.
27. Tiwari, V.S. and D. Pandey, *Structure and Properties of (Ba, Ca) TiO3 Ceramics Prepared Using (Ba, Ca) CO3 Precursors: II, Diffuse Phase Transition Behavior.* Journal of the American Ceramic Society, 1994. **77**(7): p. 1819-1824.
28. Kirillov, V. and V. Isupov, *Relaxation polarization of PbMg 1/3Nb2/3O3 (PMN)-A ferroelectric with a diffused phase transition.* Ferroelectrics, 1973. **5**(1): p. 3-9.
29. Delgado, M., *Phase Transitions in Relaxor Ferroelectrics.* 2005.
30. Viehland, D., et al., *Dipolar-glass model for lead magnesium niobate.* Physical Review B, 1991. **43**(10): p. 8316.
31. Bell, A., *Calculations of dielectric properties from the superparaelectric model of relaxors.* Journal of Physics: Condensed Matter, 1993. **5**(46): p. 8773.
32. Maiti, T., R. Guo, and A. Bhalla, *Structure-Property Phase Diagram of BaZrxTi1− xO3 System.* Journal of the American Ceramic Society, 2008. **91**(6): p. 1769-1780.
33. Yu, Z., et al., *Piezoelectric and strain properties of Ba (Ti1-xZrx) O3 ceramics.* Journal of applied physics, 2002. **92**: p. 1489-1493.
34. Singh, S., S.P. Singh, and D. Pandey, *A succession of relaxor ferroelectric transitions in Ba0. 55Sr0. 45TiO3.* Journal of Applied Physics, 2008. **103**(1): p. 6107.
35. Zhou, L., P. Vilarinho, and J. Baptista, *Dependence of the Structural and Dielectric Properties of Ba 1-x Sr x TiO 3 Ceramic Solid Solutions on Raw Material Processing.* Journal of the European Ceramic Society, 1999. **19**(11): p. 2015-2020.
36. Lemanov, V., et al., *Phase transitions and glasslike behavior in Sr 1− x Ba x TiO 3.* Physical Review B, 1996. **54**(5): p. 3151.
37. Wang, R., Y. Inaguma, and M. Itoh, *Dielectric properties and phase transition mechanisms in Sr 1− x Ba x TiO 3 solid solution at low doping concentration.* Materials research bulletin, 2001. **36**(9): p. 1693-1701.
38. Jeon, J.-H., *Effect of SrTiO 3 concentration and sintering temperature on microstructure and dielectric constant of Ba 1− x Sr x TiO 3.* Journal of the European Ceramic Society, 2004. **24**(6): p. 1045-1048.
39. Su, B. and T. Button, *Microstructure and dielectric properties of Mg-doped barium strontium titanate ceramics.* Journal of applied physics, 2004. **95**: p. 1382-1385.
40. Chang, W. and L. Sengupta, *MgO-mixed Ba0. 6Sr0. 4TiO3 bulk ceramics and thin films for tunable microwave applications.* Journal of Applied Physics, 2002. **92**(7): p. 3941-3946.
41. Remmel, T., R. Gregory, and B. Baumert, *Characterization of barium strontium titanate films using XRD.* International Centre for Diffraction Data, 1999.
42. Badapanda, T., et al., *Ferroelectric phase transition of Ba1− x Sr x Ti0. 6Zr0. 4O3 ceramics.* Phase Transitions, 2008. **81**(10): p. 897-906.
43. Bokov, A., et al., *Dielectric Behavior of Ba (Ti1− xZrx) O3 Solid Solution.* Ferroelectrics, 2006. **337**(1): p. 169-178.
44. Scott, J., *Applications of modern ferroelectrics.* science, 2007. **315**(5814): p. 954-959.
45. Reddy, S.B., K.P. Rao, and M.R. Rao, *Structural and dielectric characterization of Sr substituted Ba (Zr, Ti) O3 based functional materials.* Applied Physics A, 2007. **89**(4): p. 1011-1015.
46. Badapanda, T., et al., *Relaxor behaviour of (Ba0· 5Sr0· 5)(Ti0· 6Zr0· 4) O3 ceramics.* Bulletin of Materials Science, 2008. **31**(6): p. 897-901.
47. NACEUR, H., A. MEGRICHE, and M. EL MAAOUI, *Frequency-dependant dielectric characteristics and conductivity behavior of Sr1− x (Na0. 5Bi0. 5) xBi2Nb2O9 (x= 0.0, 0.2, 0.5, 0.8 and 1.0) ceramics.* Oriental Journal of Chemistry, 2013. **29**(3): p. 937-944.
48. Hyeon, T., et al., *Synthesis of highly crystalline and monodisperse cobalt ferrite nanocrystals.* The Journal of Physical Chemistry B, 2002. **106**(27): p. 6831-6833.
49. Kwei, G., et al., *Structures of the ferroelectric phases of barium titanate.* The Journal of Physical Chemistry, 1993. **97**(10): p. 2368-2377.

50. Shirane, G., H. Danner, and R. Pepinsky, *Neutron Diffraction Study of Orthorhombic BaTi O 3.* Physical Review, 1957. **105**(3): p. 856.